Available online at www.sciencedirect.com
SCIENCE DIRECT®
Journal of Sound and Vibration 292 (2006) 242–278
JOURNAL OF SOUND AND VIBRATION
www.elsevier.com/locate/jsvi

Dynamical behavior of vibro-impact machinery near a point of codimension two bifurcation

G.W. Luo[a,*], Y.L. Zhang[b], J.N. Yu[a]

[a]School of Mathematics, Physics and Software Engineering, Lanzhou Jiaotong University, Lanzhou, 730070, People's Republic of China
[b]School of Mechatronics Engineering, Lanzhou Jiaotong University, Lanzhou, 730070, People's Republic of China

Received 21 July 2003; received in revised form 6 May 2005; accepted 29 July 2005
Available online 8 November 2005

Abstract

A dual component system with vibro-impact is considered. Local codimension two bifurcation of maps, involving a real eigenvalue and a complex conjugate pair escaping the unit circle simultaneously, is analyzed by using the center manifold and normal form method for maps. The period n single-impact motion and Poincaré map of the vibro-impact system are derived analytically. Stability and local bifurcation of single-impact periodic motion are analyzed by using the Poincaré map. A center manifold theorem technique is applied to reduce the Poincaré map to a three-dimensional one, and the normal form map associated with the codimension two bifurcation is obtained. Local behavior of the dual component system with vibro-impact, near the point of codimension two bifurcation, is analyzed. It is found that near the point of codimension two bifurcation, there exists not only Hopf bifurcation of period one single-impact motion, but also Hopf bifurcation of period two double-impact motion. Period doubling bifurcation of period one single-impact motion commonly exists near the point of codimension two bifurcation. However, no period doubling cascade emerges due to change of the type of period two fixed points and occurrence of Hopf bifurcation associated with period two fixed points. The period two fixed points are symmetrical about the corresponding period one point. The results from simulation show that the attracting invariant circles associated with period two points are symmetrical about the corresponding period one point near the value of Hopf bifurcation of period two points. Two actual examples, the impact-forming machinery and inertial shaker, are chosen to analyze further the phenomena of codimension two bifurcation of maps, and local bifurcation analysis and numerical simulation are carried out to unfold dynamical behavior of these vibro-impact systems near the points of codimension two bifurcations.

1. Introduction

Vibrating systems with clearances, gaps or stops are frequently encountered in technical applications of mechanism, vehicle traffic, nuclear reactor, etc. Repeated impacts, i.e., vibro-impacts, usually occur whenever the components of a vibrating system collide with rigid obstacles or with each other. The principle of operation of vibration hammers, impact dampers, machinery for compacting, milling and forming, offshore structures, shakers and pile drivers, etc., is based on the impact action for moving bodies. With other

*Corresponding author.
E-mail addresses: luogw@mail.lzjtu.cn, luogw@hotmail.com (G.W. Luo).

0022-460X/$ - see front matter © 2005 Elsevier Ltd. All rights reserved.
doi:10.1016/j.jsv.2005.07.051

equipment, e.g., mechanisms with clearances, heat exchangers, fuel elements of nuclear reactors, gears, piping systems, wheel–rail interaction of high speed railway coaches, etc., impacts also occur, but they are undesirable as they bring about failures, strain, shorter service life and increased noise levels. Researches into vibro-impact problems have significance on optimization design of machinery with clearances, gaps or stops, noise suppression, reliability analyses, etc. The physical process during impacts is strongly nonlinear and discontinuous, but it can be described theoretically and numerically by discontinuities in good agreement with reality. Compared with single impact, the dynamics of vibro-impacts is more complicated, and hence, has received great attention. Many new theoretical problems have been advanced in researches into vibro-impacts dynamics, and the study of problems of impacting vibration becomes a new subject on nonlinear dynamics. Some important problems on vibro-impact dynamics, including global bifurcations [1–8], singularities [9–18], chattering impact [19], quasi-periodic impacts [20–24] controlling chaos [25], etc., have been studied in the past several years. Along with the theoretical researches into vibro-impact dynamics, the research into application of these systems are developed, for example, wheel-rail impact of railway coaches [26], impact noise analysis [27], shakers [28,29], vibrating hammer [30], offshore structure [31], impact dampers [32–36], gears [37,38], etc.

The purpose of the present study is to focus attention on codimension two bifurcation of period one single-impact motion of vibro-impact systems. There are many types of codimension two bifurcations of ordinary differential equations and maps, some of which are studied in Refs. [39–45]. Here a local codimension two bifurcation of maps, involving a real eigenvalue and a complex conjugate pair escaping the unit circle simultaneously, is analyzed by using the center manifold normal form method for maps. A dual component system with vibro-impact is considered. The period n single-impact motion and Poincaré map of the vibro-impact system are derived analytically. Stability and local bifurcation of single-impact periodic motion are analyzed by using the Poincaré map. A center manifold theorem technique is applied to reduce the Poincaré map to a three-dimensional one, and the normal form map associated with the codimension two bifurcation is obtained. Local behavior of the dual component system with vibro-impact, near the point of codimension two bifurcation, is analyzed. It is found that near the point of codimension two bifurcation there exists not only Hopf bifurcation of period one single-impact motion, but also Hopf bifurcation of period two double-impact motion. Period doubling bifurcation of period one single-impact motion is commonly existent near the point of codimension two bifurcation. However, no period doubling cascade emerges due to change of the type of period two fixed points and occurrence of Hopf bifurcation associated with period two fixed points. The period two fixed points are symmetrical about the corresponding period one point. The results from simulation show that the attracting invariant circles associated with period two points are symmetrical about the corresponding period one point near the value of Hopf bifurcation of period two points. Finally, two actual examples, the impact-forming machinery and inertial shaker, are chosen to analyze further the phenomena of codimension two bifurcation of impact maps, and local bifurcation analysis and numerical simulation are carried out to unfold dynamical behavior of these vibro-impact systems near the points of codimension two bifurcations.

2. The mechanical models of vibro-impact systems

The mechanical models for a dual component system with vibro-impact, the impact-forming machinery and inertial shaker are shown, respectively, in Figs. 1(a), (b) and (c). We first analyze the dual component system shown in Fig. 1(a). Displacements of the masses M_1 and M_2 are represented by X_1 and X_2, respectively. The masses are connected to the supporting base by the linear springs with stiffnesses K_1 and K_2, and linear viscous dashpots with damping constants C_1 and C_2. The excitations on masses are harmonic with amplitudes P_1 and P_2. Ω is the excitation frequency, and τ is the phase angle. The mass M_1 impacts mutually with the mass M_2 when the difference of their displacements equals the gap Δ, i.e. $X_1(t)-X_2(t) = \Delta$. The impact is described by the conservation law of momentum and a coefficient of restitution R, and it is assumed that the duration of impact is negligible compared to the period of the force.

The motion process of the system, between any two consecutive impacts, is considered. Between any two consecutive impacts, the time T is always set to zero directly at the instant when the former impact is over, and the phase angle τ is used only to make a suitable choice for the origin of time in the calculation. The state of the vibro-impact system, immediately after impact, has become initial conditions in the subsequent process of

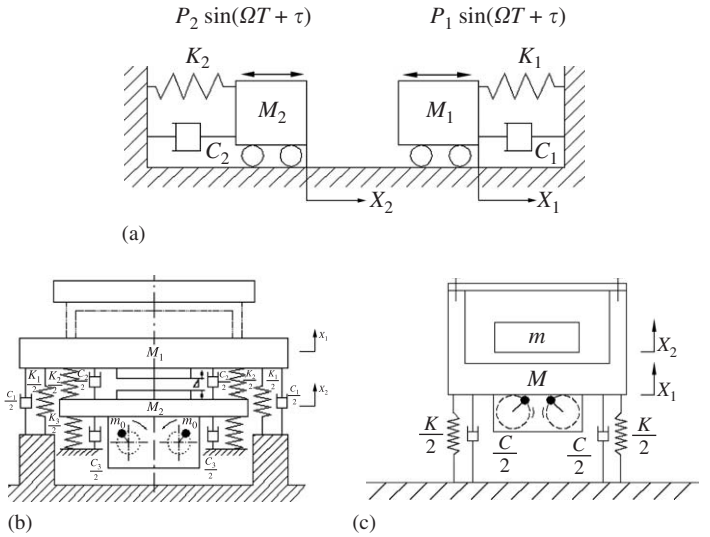

Fig. 1. Schematics of the vibro-impacts systems. (a) A dual component system with vibro-impact, (b) the impact-forming machinery, and (c) the inertial shaker.

the motion. Between consecutive impacts, the non-dimensional differential equations of motion are given by

$$\ddot{x}_1 + 2\zeta_1\dot{x}_1 + x_1 = \sin(\omega t + \tau), \quad \ddot{x}_2 + 2\zeta_2\omega_0\dot{x}_2 + \omega_0^2 x_2 = f_0\sin(\omega t + \tau), \tag{1}$$

where a dot $(\cdot)$ denotes differentiation with respect to the non-dimensional time t, and the non-dimensional quantities are given by

$$\mu_m = \frac{M_1}{M_2}, \quad \zeta_i = \frac{C_i}{2\sqrt{K_i M_i}}, \quad x_i = \frac{X_i K_1}{P_1}, \quad i = 1, 2$$
$$f_0 = \frac{\mu_m P_2}{P_1}, \quad \omega_0 = \sqrt{\frac{K_2\mu_m}{K_1}}, \quad \omega = \Omega\sqrt{\frac{M_1}{K_1}}, \quad t = T\sqrt{\frac{K_1}{M_1}}, \quad \delta = \frac{\Delta\cdot K_1}{P_1}. \tag{2}$$

When the impact occurs, for $x_1(t) - x_2(t) = \delta$, the velocities of the masses M_1 and M_2 are changed according to the conservation law of momentum, and the impact equation of the masses and the coefficient of restitution R are given by

$$\mu_m\dot{x}_{1+} + \dot{x}_{2+} = \mu_m\dot{x}_{1-} + \dot{x}_{2-}, \quad R = (\dot{x}_{2+} - \dot{x}_{1+})/(\dot{x}_{1-} - \dot{x}_{2-}), \tag{3}$$

where $\dot{x}_{i-}$ and $\dot{x}_{i+}$ $(i = 1, 2)$ represent the velocities of immediately before and after the impact of the masses M_i, respectively.

The general solutions of Eq. (1) are given by

$$x_j(t) = \mathrm{e}^{-\eta_j t}(a_j\cos\omega_{dj}t + b_j\sin\omega_{dj}t) + A_j\sin(\omega t + \tau) + B_j\cos(\omega t + \tau) \quad (j = 1, 2), \tag{4}$$

where $\eta_1 = \zeta_1$, $\eta_2 = \zeta_2\omega_0$, $\omega_{d1} = \sqrt{1-\zeta_1^2}$, $\omega_{d2} = \omega_0\sqrt{1-\zeta_2^2}$, a_j and b_j are the constants of integration which are determined by the initial condition and modal parameters of the system, and A_j and B_j are the amplitude constants.

3. Single-impact periodic motion

Impacting systems are conveniently studied using a mapping derived from the equations of motion. Each iterate of this map corresponds to the mass M_1 striking the mass M_2 once. In this section, only the periodic motion of the model, with one impact during n cycles of the force, is considered, which is called the period n

single-impact motion. Letting $\theta = \omega t$, there are generally two ways to choose the Poincaré sections: $\bar{\sigma}, \sigma \subset \mathbf{R}^4 \times \mathbf{S}$, where $\bar{\sigma} = \{(x_1, \dot{x}_1, x_2, \dot{x}_2, \theta) \in \mathbf{R}^4 \times \mathbf{S},\ \theta = 0,\ \mathrm{mod}(2\pi)\}$, $\sigma = \{(x_1, \dot{x}_1, x_2, \dot{x}_2, \theta) \in \mathbf{R}^4 \times \mathbf{S},\ x_1 - x_2 = \delta,\ \dot{x}_1 = \dot{x}_{1+}, \dot{x}_2 = \dot{x}_{2+}\}$. Because there exists singularity of the Poincaré map caused by the motions with grazing contact of two masses in the vibro-impact systems, it is difficult to observe the motions with grazing contact of two masses in the Poincaré section $\bar{\sigma}$. In this paper, we choose the section σ to establish the Poincaré map of the system. The disturbed map of period n single-impact motion is expressed as

$$X' = f(v, X), \tag{5}$$

where $X \in \mathbf{R}^4$, v is varying parameters, $v \in \mathbf{R}^1$ or $\mathbf{R}^2$; $X = X^* + \Delta X$, $X' = X^* + \Delta X'$, $X^* = (\dot{x}_{1+}, x_{20}, \dot{x}_{2+}, \tau_0)^{\mathrm{T}}$ is a fixed point in the hyperplane σ, $\Delta X = (\Delta\dot{x}_{1+}, \Delta x_{20}, \Delta\dot{x}_{2+}, \Delta\tau)^{\mathrm{T}}$ and $\Delta X' = (\Delta\dot{x}'_{1+}, \Delta x'_{20}, \Delta\dot{x}'_{2+}, \Delta\tau')^{\mathrm{T}}$ are the disturbed vectors of X^*.

Under suitable system parameter conditions, the system shown in Fig. 1(a) exhibits periodic behavior. In the paper, we can characterize periodic impact motions of the vibro-impact system by the symbol $q = p/n$, where p is the number of impacts and n is the number of the forcing cycle. The symbol q, originated by F. Peterka, is of significance in analyzing the periodic-impact motions and bifurcation characteristics, and the quantity q has rational and irrational value for periodic and chaotic motion, respectively; see Ref. [15]. The $q = 1/n$ motion means that if the dimensionless time t is set to zero directly after an impact, then it becomes $2n\pi/\omega$ $(n = 1, 2, \ldots)$ just before the next impact. After the origin of θ-coordinate is displaced to an impact point, the determination of the periodic motion is based on the fact that they satisfy the following set of periodicity and matching conditions:

$$x_1(0) = x_1(2n\pi/\omega) = x_{10},\ \ x_2(0) = x_2(2n\pi/\omega) = x_{20},$$

$$x_1(0) - x_2(0) = \delta,\ \ x_1(2n\pi/\omega) - x_2(2n\pi/\omega) = \delta,$$

$$\dot{x}_1(0) = \frac{1}{1+\mu_m}\left[(\mu_m - R)\dot{x}_1(2n\pi/\omega) + (1+R)\dot{x}_2(2n\pi/\omega)\right] = \dot{x}_{1+},$$

$$\dot{x}_2(0) = \frac{1}{1+\mu_m}\left[\mu_m(1+R)\dot{x}_1(2n\pi/\omega) + (1 - R\mu_m)\dot{x}_2(2n\pi/\omega)\right] = \dot{x}_{2+}, \tag{6}$$

where $\dot{x}_1(2n\pi/\omega) = \dot{x}_{1-}$ and $\dot{x}_2(2n\pi/\omega) = \dot{x}_{2-}$, respectively, are the velocities of masses M_1 and M_2 immediately before the impact.

Inserting the set of periodicity and matching conditions (6) into the general solutions of Eq. (1), we can solve for the constants of integration a_j, b_j and the phase angle τ_0 from the formula (4). For convenience, in the following, we give expressions for some symbols h, l_j and $\bar{l}_j$, firstly:

$$l_j = \frac{R\omega_{dj}e_j(c_j - e_j) - (R+1)e_j\eta_j s_j}{1 - e_j c_j} + \omega_{dj}, \quad \bar{l}_j = \frac{\omega_{dj}e_j(e_j - c_j)}{1 - e_j c_j} + \omega_{dj}, \quad (j = 1, 2),$$

$$h = -\left(\frac{\bar{l}_2\omega(1+R)}{\mu_m\bar{l}_1 l_2 + l_1\bar{l}_2}\right)\left(\frac{e_1 s_1}{1 - e_1 c_1} + \frac{e_2 s_2}{1 - e_2 c_2}\frac{\bar{l}_1\mu_m}{\bar{l}_2}\right), \tag{7}$$

where $s_j = \sin(2n\pi\omega_{dj}/\omega)$, $c_j = \cos(2n\pi\omega_{dj}/\omega)$, $e_j = \mathrm{e}^{-\eta_j 2n\pi/\omega}$, $j = 1, 2$.

The phase angle and constants of integration of $q = 1/n$ motion are given by

$$\tau_0 = \cos^{-1}\left(\frac{\bar{\delta}\gamma \pm \sqrt{\gamma^2 - \bar{\delta}^2 + 1}}{\gamma^2 + 1}\right), \tag{8}$$

$$b_1 = \frac{\bar{l}_2\omega(R+1)(d_2\sin\tau_0 - d_1\cos\tau_0)}{\mu_m\bar{l}_1 l_2 + l_1\bar{l}_2}, \quad b_2 = \frac{\mu_m\bar{l}_1\omega(R+1)(d_1\cos\tau_0 - d_2\sin\tau_0)}{l_1\bar{l}_2 + \bar{l}_1 l_2\mu_m}, \tag{9}$$

$$a_j = \frac{e_j b_j s_j}{1 - e_j c_j}, \quad (j = 1, 2). \tag{10}$$

In the formula (8)

$$\gamma = \frac{hd_1 + d_2}{hd_2 - d_1}, \quad d_1 = A_1 - A_2, \quad d_2 = B_1 - B_2, \quad \bar{\delta} = \frac{\delta}{hd_2 - d_1},$$

the sign $\pm$ means that it is possible for two different single-impact periodic solutions to exist under the same system parameters for the vibro-impact system. It should be noted that the existence of period n single-impact orbit requires the condition as given below:

$$\gamma^2 - \bar{\delta}^2 + 1 \geqslant 0, \quad \left| \frac{\bar{\delta}\gamma \pm \sqrt{\gamma^2 - \bar{\delta}^2 + 1}}{\gamma^2 + 1} \right| \leqslant 1, \tag{11}$$

otherwise, it is impossible for single-impact periodic motions to exist. Substituting the constants of integration (8)–(10) into the general solutions of Eq. (1), we obtain the periodic solutions, which correspond to one impact during n cycles of the forcing. Inserting the time $t = 0$ into the periodic solution, we can obtain the fixed point $X^* = (\dot{x}_{1+}, x_{20}, \dot{x}_{2+}, \tau_0)^{\mathrm{T}}$, which is the projection of period n single-impact orbit to Poincaré section σ.

4. Stability and local bifurcation of single-impact periodic motion

If the $q = 1/n$ periodic motion is disturbed at the instant of impact by the differences $\Delta\dot{x}_{1+}$, Δx_{20}, $\Delta\dot{x}_{2+}$ and $\Delta\tau$, then one can express the differences $\Delta\dot{x}'_{1+}$, $\Delta x'_{20}$, $\Delta\dot{x}'_{2+}$ and $\Delta\tau'$ at the next impact. Here $\tilde{X} = (\tilde{x}_1, \tilde{x}_2)^{\mathrm{T}}$ and $\dot{\tilde{X}} = (\dot{\tilde{x}}_1, \dot{\tilde{x}}_2)^{\mathrm{T}}$ represent displacements and velocities of the disturbed motion, respectively. The solutions of disturbed motion between two consecutive impacts are given by

$$\tilde{x}_j(t) = \mathrm{e}^{-\eta_j t}(\tilde{a}_j \cos\omega_{dj} t + \tilde{b}_j \sin\omega_{dj} t) + A_j \sin(\omega t + \tau_0 + \Delta\tau) + B_j \cos(\omega t + \tau_0 + \Delta\tau), \quad j = 1, 2. \tag{12}$$

For the disturbed motion, the dimensionless time is set to zero directly after an impact, it becomes $(2n\pi + \Delta\theta)/\omega$ just before the next impact, and $\Delta\theta = \Delta\tau' - \Delta\tau$. Letting $t_e = (2n\pi + \Delta\theta)/\omega$, the boundary conditions at two successive impact points are given by

$$\tilde{x}_i(0) = x_{i0} + \Delta x_{i0}, \quad \tilde{x}_i(t_e) = x_{i0} + \Delta x'_{i0}, \quad \dot{\tilde{x}}_i(0) = \dot{x}_{i+} + \Delta\dot{x}_{i+}, \quad \dot{\tilde{x}}_i(t_{e-}) = \dot{x}_{i-} + \Delta\dot{x}'_{i-},$$

$$\dot{\tilde{x}}_i(t_{e+}) = \dot{x}_{i+} + \Delta\dot{x}'_{i+}, \quad i = 1, 2; \quad \tilde{x}_1(0) - \tilde{x}_2(0) = \tilde{x}_1(t_e) - \tilde{x}_2(t_e) = \delta;$$

$$\dot{\tilde{x}}_1(t_{e+}) = \frac{1}{1 + \mu_m}\left[(\mu_m - R)\dot{\tilde{x}}_1(t_{e-}) + (1 + R)\dot{\tilde{x}}_2(t_{e-})\right] = \dot{x}_{1+} + \Delta\dot{x}'_{1+},$$

$$\dot{\tilde{x}}_2(t_{e+}) = \frac{1}{1 + \mu_m}\left[\mu_m(1 + R)\dot{\tilde{x}}_1(t_{e-}) + (1 - R\mu_m)\dot{\tilde{x}}_2(t_{e-})\right] = \dot{x}_{2+} + \Delta\dot{x}'_{2+}, \tag{13}$$

where t_{e-} and t_{e+} represent, respectively, the time shortly before and after the instant of impact.

Inserting the boundary condition (13) into the disturbed solution (12) for $t = 0$, we can solve

$$\tilde{a}_1 = \delta + x_{20} + \Delta x_{20} - A_1 \sin(\tau_0 + \Delta\tau) - B_1 \cos(\tau_0 + \Delta\tau), \tag{14}$$

$$\tilde{a}_2 = x_{20} + \Delta x_{20} - A_2 \sin(\tau_0 + \Delta\tau) - B_2 \cos(\tau_0 + \Delta\tau), \tag{15}$$

$$\tilde{b}_1 = \frac{1}{\omega_{d1}}\left[\dot{x}_{1+} + \Delta\dot{x}_{1+} + \eta_1\delta + \eta_1(x_{20} + \Delta x_{20}) - (A_1\omega + B_1\eta_1)\cos(\tau_0 + \Delta\tau) + (B_1\omega - A_1\eta_1)\sin(\tau_0 + \Delta\tau)\right], \tag{16}$$

$$\tilde{b}_2 = \frac{1}{\omega_{d2}}[\dot{x}_{2+} + \Delta\dot{x}_{2+} + \eta_2(x_{20} + \Delta x_{20}) - (A_2\omega + B_2\eta_2)\cos(\tau_0 + \Delta\tau) + (B_2\omega - A_2\eta_2)\sin(\tau_0 + \Delta\tau)]. \tag{17}$$

Inserting the boundary condition (13) into the disturbed solution (12) for $t = t_e$, we can obtain

$$\tilde{x}_1(t_e) - \tilde{x}_2(t_e) = \delta, \quad \dot{x}_{1+} + \Delta\dot{x}'_{1+} = \frac{\mu_m - R}{\mu_m + 1}\dot{\tilde{x}}_1(t_e) + \frac{R+1}{\mu_m+1}\dot{\tilde{x}}_2(t_e), \quad x_{20} + \Delta x'_{20} = \tilde{x}_2(t_e),$$

$$\dot{x}_{2+} + \Delta\dot{x}'_{2+} = \frac{\mu_m R + \mu_m}{\mu_m + 1}\dot{\tilde{x}}_1(t_e) + \frac{1 - \mu_m R}{\mu_m + 1}\dot{\tilde{x}}_2(t_e),$$

$$\tau' = \tau_0 + \Delta\tau' = \tau_0 + \Delta\tau + \Delta\theta(\Delta\dot{x}_{1+}, \Delta x_{20}, \Delta\dot{x}_{2+}, \Delta\tau). \tag{18}$$

Defining a function $g(\Delta\dot{x}_{1+}, \Delta x_{20}, \Delta\dot{x}_{2+}, \Delta\tau, \Delta\theta)$ as

$$g(\Delta\dot{x}_{1+}, \Delta x_{20}, \Delta\dot{x}_{2+}, \Delta\tau, \Delta\theta) = \tilde{x}_1(t_e) - \tilde{x}_2(t_e) - \delta. \tag{19}$$

The condition, under which there exists $q = 1/n$ fixed point, leads to the formula

$$g(\Delta\dot{x}_{1+}, \Delta x_{20}, \Delta\dot{x}_{2+}, \Delta\tau, \Delta\theta)\big|_{(0,0,0,0,0)} = 0. \tag{20}$$

Supposing $\left(\partial g/\partial\Delta\theta\right)_{(0,0,0,0,0)} \neq 0$, using the implicit function theorem and solving Eq. (20) for $\Delta\theta$, one obtains

$$\Delta\theta = \Delta\theta(\Delta\dot{x}_{1+}, \Delta x_{20}, \Delta\dot{x}_{2+}, \Delta\tau), \quad \Delta\theta(0,0,0,0) = 0. \tag{21}$$

Inserting formula (21) into Eq. (18), we finally get the Poincaré map of periodic impact, which is given by

$$X' = f(v, X), \tag{22}$$

where $\Delta X = (\Delta\dot{x}_{1+}, \Delta x_{20}, \Delta\dot{x}_{2+}, \Delta\tau)^{\mathrm{T}}$, $\Delta X' = (\Delta\dot{x}'_{1+}, \Delta x'_{20}, \Delta\dot{x}'_{2+}, \Delta\tau')^{\mathrm{T}}$, $X = X^* + \Delta X$, $X' = X^* + \Delta X'$, $X^* = (\dot{x}_{1+}, x_{20}, \dot{x}_{2+}, \tau_0)^{\mathrm{T}}$.

Linearizing the Poincaré map at the fixed point results in the matrix (Jacobian matrix), we have

$$\mathrm{D}f(v, X^*) = \left.\frac{\partial f(v, X)}{\partial X}\right|_{(v, X^*)}. \tag{23}$$

If the map $f(v, X)$ has a fixed point, then the vibro-impact system shown in Fig. 1(a) has a $q = 1/n$ impact orbit. If none of the eigenvalues of Jacobian matrix $\mathrm{D}f(v_0, X^*)$ lies on the unit circle or outside it, then it can be shown that $f(v, X)$ has essentially the same behavior as $f(v_0, X)$ for $|v - v_0|$ small. Suppose that for $v = v_0$, the system has a stable periodic solution $X^*(t)$ with period $2n\pi/\omega$. Hence in this case, for $|v - v_0|$ small, the solutions of the vibro-impact system near $X^*(t)$ have a stable periodic behavior as $v = v_0$. The stability and local bifurcation of $q = 1/n$ impact motion are determined by computing eigenvalues of $\mathrm{D}f(v, X^*)$. If the eigenvalues of $\mathrm{D}f(v, X^*)$ with the largest modules lie on the unit circle when $v = v_c$ (v_c is a bifurcation value) then there is the possibility of bifurcations taking place. In general, bifurcations occur in various ways according to the numbers of the eigenvalues on the unit circle and their position on the unit circle, resulting in qualitative changes of the system dynamics. If Jacobian matrix $\mathrm{D}f(v, X^*)$ has a pair of complex conjugate eigenvalues, crossing the unit circle as v passes v_c; the remainder of the spectrum of $\mathrm{D}f(v, X^*)$ will be assumed to stay strictly inside the unit circle, then it is very likely that Hopf bifurcation associated with $q = 1/n$ motion takes place. If the Jacobian matrix $\mathrm{D}f(v, X^*)$ has a real eigenvalue, crossing the unit circle from the point $(-1, 0)$ or the point $(+1, 0)$ as v passes v_c, the remainder of the spectrum of $\mathrm{D}f(v, X^*)$ are strictly inside the unit circle, period-doubling or saddle-node bifurcation of $q = 1/n$ motion can occur, respectively. Moreover, we shall also consider the case of $v \in \mathbf{R}^2$, and the dynamics of the system is studied with special attention to codimension two bifurcation of $q = 1/1$ motion.

There exist six cases of codimension two bifurcations of maps, i.e., the double eigenvalues $\lambda_1(v_c) = \lambda_2(v_c) = -1$, $\lambda_1(v_c) = \lambda_2(v_c) = 1$; $\lambda_1(v_c) = -1$, $\lambda_2(v_c) = 1$; a real eigenvalue $\lambda_1(v)$ and a complex conjugate pair of eigenvalues $\lambda_{2,3}(v)$ escaping the unit circle simultaneously, $\lambda_1(v_c) = -1$ or 1, $|\lambda_{2,3}(v_c)| = 1$; two complex conjugate pairs of eigenvalues escaping the unit circle simultaneously, $|\lambda_{1,2}(v_c)| = 1$, $|\lambda_{3,4}(v_c)| = 1$. Here we consider only a case in which a complex conjugate pair of eigenvalues and a real eigenvalue escape the unit circle simultaneously.

5. The center manifold and normal form map

We continue to consider the Poincaré map $X' = f(v, X)$. X^* is a fixed point for the map for v in some neighborhood of a critical value $v = v_c$ at which $Df(v, X^*)$ satisfies the following assumptions:

H1. Jacobian matrix $Df(v, X^*)$ has eigenvalues $\lambda_1(v_c)$, $\lambda_2(v_c)$ and $\lambda_3(v_c)$ on the unit circle, in which $\lambda_1(v_c)$ is a real eigenvalue and $\lambda_{2,3}(v_c)$ are a pair of complex conjugate eigenvalues, and $\lambda_1(v_c) = -1$, $\lambda_2(v_c) = \bar{\lambda}_3(v_c)$, $|\lambda_{2,3}(v_c)| = 1$.

H2. The remainder of the spectrum of $Df(v, X^*)$ are strictly inside the unit circle.

For all v in some neighborhood of v_c, the map (22), under the change of variables $\mu_1 = v_1 - v_{1c}$, $\mu_2 = v_2 - v_{2c}$, $\mu = (\mu_1, \mu_2)^{\mathrm{T}}$ and $X = X^* + P\tilde{Y}$, becomes

$$\tilde{Y}' = \tilde{F}(\mu; \tilde{Y}), \tag{24}$$

where P is the eigenmatrix [23], $\tilde{Y} = (y_1, y_2, y_3, y_4)^{\mathrm{T}}$, $\tilde{F} = (F_1, F_2, F_3, F_4)^{\mathrm{T}}$.

Letting $z_1 = y_1$, $z_2 = y_2 + \mathrm{i}y_3$, $\bar{z}_2 = y_2 - \mathrm{i}y_3$, $z = (z_1, z_2, \bar{z}_2)^{\mathrm{T}}$, $W = y_4$, $G_1 = F_1 - \lambda_1 z_1$, $G_2 = F_2 + \mathrm{i}F_3 - \lambda_2 z_2$ and $H = F_4 - \lambda_4 W$, the map (24) may be expressed by

$$\begin{aligned} z_1' &= \lambda_1 z_1 + G_1(z_1, z_2, \bar{z}_2, W; \mu), \quad z_2' = \lambda_2 z_2 + G_2(z_1, z_2, \bar{z}_2, W; \mu), \\ W' &= \lambda_4 W + H(z_1, z_2, \bar{z}_2, W; \mu), \end{aligned} \tag{25}$$

in which $\lambda_1 = \tilde{\lambda}_1(\mu) = \lambda_1(v_c + \mu)$, $\lambda_2 = \tilde{\lambda}_2(\mu) = \lambda_2(v_c + \mu)$, $\tilde{\lambda}_1(0) = -1$, $\tilde{\lambda}_{2,3}(0) = \alpha \pm \mathrm{i}\varpi$, $|\tilde{\lambda}_{2,3}(0)| = 1$. For the map (25), there exists a local center manifold $W(z_1, z_2, \bar{z}_2; \mu)$ [44,46], which may be determined by the equation

$$W(z_1', z_2', \bar{z}_2'; \mu) = \lambda_4 W(z_1, z_2, \bar{z}_2; \mu) + H(z_1, z_2, \bar{z}_2, W(z_1, z_2, \bar{z}_2; \mu); \mu). \tag{26}$$

On the center manifold the local behavior of the map (25) can be reduced to a three-dimensional map $\tilde{\Phi}(z; \mu)$, which is now

$$\begin{aligned} z_1' &= \tilde{\lambda}_1(\mu) z_1 + G_1(z_1, z_2, \bar{z}_2, W(z_1, z_2, \bar{z}_2; \mu); \mu), \\ z_2' &= \tilde{\lambda}_2(\mu) z_2 + G_2(z_1, z_2, \bar{z}_2, W(z_1, z_2, \bar{z}_2; \mu); \mu), \end{aligned} \tag{27}$$

where the Taylor series expansion of $W(z_1, z_2, \bar{z}_2; \mu)$ and $G_i(z_1, z_2, \bar{z}_2, W(z_1, z_2, \bar{z}_2; \mu); \mu)$ about $(0,0,0,\mu)$ may be determined by the method which is given in Appendix A.

The three-dimensional map has the following form $\tilde{\Phi}(z; \varepsilon)$:

$$\begin{aligned} z_1' &= \tilde{\lambda}_1(\mu) z_1 + \sum_{i+j+k=2}^{3} g_{ijk}^{(1)}(\mu) \frac{z_1^i z_2^j \bar{z}_2^k}{i!j!k!} + \left(O(|z_1| + |z_2|)^4\right), \\ z_2' &= \tilde{\lambda}_2(\mu) z_2 + \sum_{i+j+k=2}^{3} g_{ijk}^{(2)}(\mu) \frac{z_1^i z_2^j \bar{z}_2^k}{i!j!k!} + \left(O(|z_1| + |z_2|)^4\right). \end{aligned} \tag{28}$$

By using the center manifold technique and normal form method of maps, we can reduce the map (28) to the normal form map $\Phi(z; \varepsilon)$, which is given by

$$\begin{aligned} z_1' &= -z_1 + \varepsilon_1 z_1 + a z_1^3 + b z_1 |z_2|^2 + O\left((|z_1| + |z_2|)^5\right), \\ z_2' &= \tilde{\lambda}_2(0) z_2 + \tilde{\varepsilon}_2 z_2 + \tilde{c} z_1^2 z_2 + \tilde{d} z_2 |z_2|^2 + O\left((|z_1| + |z_2|)^5\right). \end{aligned} \tag{29}$$

The normal form map (29), in the real form $\Phi(Y; \varepsilon)$, is expressed by

$$\begin{aligned} y_1' &= -y_1 + \varepsilon_1 y_1 + a y_1^3 + b y_1 (y_2^2 + y_3^2) + \text{h.o.t}, \\ y_2' &= (\alpha + \varepsilon_2) y_2 - (\varpi + \varepsilon_3) y_3 + (c y_2 - e y_3) y_1^2 + (d y_2 - f y_3)(y_2^2 + y_3^2) + \text{h.o.t}, \\ y_3' &= (\varpi + \varepsilon_3) y_2 + (\alpha + \varepsilon_2) y_3 + (c y_3 + e y_2) y_1^2 + (d y_3 + f y_2)(y_2^2 + y_3^2) + \text{h.o.t}, \end{aligned} \tag{30}$$

in which, $\varepsilon = (\varepsilon_1, \varepsilon_2, \varepsilon_3)^{\mathrm{T}}$, $\varepsilon_i = \varepsilon_i(\mu)$, $\varepsilon_i(0) = 0$.

6. Local codimension two bifurcation of the normal form map

6.1. A Simplified map

Let us assume that there exist period two fixed points for the normal form map $\Phi(Y;\varepsilon)$. In view of the normal form map (30), the period two points $Y_1^{(2)}$ and $Y_2^{(2)}$ satisfy the equation

$$\Phi^2(Y_i^{(2)};\varepsilon) = Y_i^{(2)}. \tag{31}$$

Ignoring the terms of high order of ε, the solutions of Eq. (31) become

$$Y_1^{(2)} = \left(\sqrt{\frac{\varepsilon_1}{-a}}, 0, 0\right)^{\mathrm{T}}, \quad Y_2^{(2)} = \left(-\sqrt{\frac{\varepsilon_1}{-a}}, 0, 0\right)^{\mathrm{T}}. \tag{32}$$

If $\varepsilon_1/a<0$, there exist the period two points $Y^{(2)} = (Y_1^{(2)}, Y_2^{(2)})^{\mathrm{T}}$, and they are symmetrical about the origin. The linearized maps of $\Phi(Y;\varepsilon)$ at the fixed point and $\Phi^2(Y;\varepsilon)$ at the period two points, respectively, are given by

$$\begin{aligned} Q_1 &= \left.\frac{\partial \Phi(Y;\ \varepsilon)}{\partial Y}\right|_{(Y_0^{(1)},\ \varepsilon)} = \begin{bmatrix} -1+\varepsilon_1 & 0 & 0 \\ 0 & \alpha+\varepsilon_2 & -\varpi-\varepsilon_3 \\ 0 & \varpi+\varepsilon_3 & \alpha+\varepsilon_2 \end{bmatrix}, \\ Q_2 &= \left.\frac{\partial \Phi^2(Y;\ \varepsilon)}{\partial Y}\right|_{(Y_i^{(2)},\ \varepsilon)} = \begin{bmatrix} 1+4\varepsilon_1 & 0 & 0 \\ 0 & q_{22} & q_{23} \\ 0 & q_{32} & q_{33} \end{bmatrix}, \end{aligned} \tag{33}$$

in which, $Y_0^{(1)} = (0,0,0)^{\mathrm{T}}$ is the trivial fixed point of normal form map (30),

$$\begin{aligned} &q_{22} = \alpha^2 - \varpi^2 + \frac{2(e\varpi - c\alpha)}{a}\varepsilon_1 + 2\alpha\varepsilon_2 - 2\varpi\varepsilon_3, \quad q_{23} = -2\varpi\alpha + \frac{2(c\varpi + e\alpha)}{a}\varepsilon_1 - 2\varpi\varepsilon_2 - 2\alpha\varepsilon_3, \\ &q_{32} = -q_{23}, \quad q_{33} = q_{22}. \end{aligned}$$

The partial bifurcation sets for the normal form map can be determined by computing and analyzing the eigenvalues of the Jacobian matrices (33). However, a full understanding of the normal form map (30) requires more than Jacobian matrices (33). So it is necessary to change the normal form map to the polar coordinate form $\Phi(r,\theta,\varepsilon_0)\in\mathbf{R}^2\times\mathbf{S}$, $(x,r,\theta)\to(x',r',\theta')$.

Letting $\tilde{\varepsilon}_2 = \tilde{\lambda}_2(0)\tilde{\varepsilon}_{20}$, $\tilde{c} = \tilde{\lambda}_2(0)\tilde{c}_0$, $\tilde{d} = \tilde{\lambda}_2(0)\tilde{d}_0$, the normal form map (29) becomes

$$\begin{aligned} z_1' &= -z_1\left(1-\varepsilon_1 - az_1^2 - b|z_2|^2\right) + O\left((|z_1|+|z_2|)^5\right), \\ z_2' &= \tilde{\lambda}_2(0)z_2\left(1+\tilde{\varepsilon}_{20} + \tilde{c}_0 z_1^2 + \tilde{d}_0|z_2|^2\right) + O\left((|z_1|+|z_2|)^5\right). \end{aligned} \tag{34}$$

In polar coordinates, the map $\Phi(z;\varepsilon_0)\in\mathbf{R}^3$ is changed to $\Phi(x;r;\theta;\varepsilon_0)\in\mathbf{R}^2\times\mathbf{S}$, which is given by

$$\begin{aligned} x' &= -x(1-\varepsilon_1 - ax^2 - br^2) + \text{h.o.t}, \\ r' &= r(1+\varepsilon_{20} + c_0x^2 + d_0r^2) + \text{h.o.t}, \\ \theta' &= \theta + \theta_0 + \varepsilon_{30} + e_0x^2 + f_0r^2 + \text{h.o.t}, \end{aligned} \tag{35}$$

in which $\varepsilon_{20} = \alpha\varepsilon_2 + \varpi\varepsilon_3$, $\varepsilon_{30} = \alpha\varepsilon_3 - \varpi\varepsilon_2$, $c_0 = \alpha c + \varpi e$, $d_0 = \alpha d + \varpi f$, $e_0 = \alpha e - \varpi c$, $f_0 = \alpha f - \varpi d$.

We ignore the influence of phase angle θ to the map (35) temporarily. By the map (35), a two-dimensional map is obtained, which is

$$\begin{aligned} x' &= -x(1-\varepsilon_1 - ax^2 - br^2) + \text{h.o.t}, \\ r' &= r(1+\varepsilon_{20} + c_0x^2 + d_0r^2) + \text{h.o.t}. \end{aligned} \tag{36}$$

Letting the iterated map $\hat{\Phi}^2(x,r;\varepsilon_0)=\left(x^{(2)},r^{(2)};\varepsilon_0\right)^{\mathrm{T}}$, then we can write

$$\begin{aligned} x^{(2)} &= x+2(-x\varepsilon_1-ax^3-bxr^2)+\text{h.o.t},\\ r^{(2)} &= r+2(r\varepsilon_{20}+c_0x^2r+d_0r^3)+\text{h.o.t.} \end{aligned} \tag{37}$$

The map (36) has two fixed points

$$Y_0=(0,0)^{\mathrm{T}},\quad Y_1^*=\left(0,\sqrt{-\varepsilon_{20}/d_0}\right)^{\mathrm{T}}.$$

The map (37) has two pairs of fixed points $Y_{21}^*=\left(\sqrt{-\varepsilon_1/a},0\right)^{\mathrm{T}}$, $Y_{22}^*=\left(-\sqrt{-\varepsilon_1/a},0\right)^{\mathrm{T}}$;

$$Y_{31}^*=\left(\sqrt{\frac{b\varepsilon_{20}-d_0\varepsilon_1}{ad_0-bc_0}},\sqrt{\frac{c_0\varepsilon_1-a\varepsilon_{20}}{ad_0-bc_0}}\right)^{\mathrm{T}},\quad Y_{32}^*=\left(-\sqrt{\frac{b\varepsilon_{20}-d_0\varepsilon_1}{ad_0-bc_0}},\sqrt{\frac{c_0\varepsilon_1-a\varepsilon_{20}}{ad_0-bc_0}}\right)^{\mathrm{T}}.$$

6.2. Simple case (I)

Two simple cases and a complex case are considered. We first analyze the unfolding of the simple case (I) associated with a scheme of coefficients of high order terms: $a>0$, $b>0$, $c_0<0$, $d_0<0$, $ad_0-bc_0<0$, $a+c_0>0$, and $b+d_0>0$. Stable conditions of these fixed points can be determined by computing and analyzing of eigenvalues of corresponding Jacobian matrices, respectively.

$Y_0=(0,0)^{\mathrm{T}}$ is the trivial fixed point of map (36), local stable condition of which is $\varepsilon_1>0$ and $\varepsilon_{20}<0$. It should be noted that the existence of the fixed point $Y_1^*=(0,\sqrt{-\varepsilon_{20}/d_0})^{\mathrm{T}}$ requires the condition $\varepsilon_{20}/d_0<0$. Local stable condition of the fixed point Y_1^* is $\varepsilon_1>b\varepsilon_{20}/d_0$ and $\varepsilon_{20}>0$. The existence of the fixed points $Y_{2i}^*=\left(\pm\sqrt{-\varepsilon_1/a},0\right)^{\mathrm{T}}$ $i=(1,2)$ requires the condition $\varepsilon_1/a<0$, and local stable condition of the fixed points Y_{2i}^* is $\varepsilon_1<0$ and $\varepsilon_{20}<c_0\varepsilon_1/a$. The existence of the fixed points Y_{3i}^* requires conditions $(b\varepsilon_{20}-d_0\varepsilon_1)/(ad_0-bc_0)>0$ and $(c_0\varepsilon_1-a\varepsilon_{20})/(ad_0-bc_0)>0$, the local stable conditions of the fixed points Y_{3i}^* are $\varepsilon_{20}>c_0\varepsilon_1/a$ and $\varepsilon_{20}<d_0(a+c_0)\varepsilon_1/(ad_0+ab)$.

Local behavior of the map (36) is not only determined by ε_1 and ε_{20}, but also by the coefficients of high order terms of the map. Now we consider the influence of phase angle θ to the map (35). By making a comparison between the map (36) and normal form map, we can unfold qualitative analyses for the normal form map. The fixed point Y_1^* of the map (36) corresponds to the invariant circle of the normal form map (30), which is associated with the fixed point $Y_0^{(1)}=(0,0,0)^{\mathrm{T}}$. The fixed points Y_{2i}^* of the map (36) correspond to period two fixed points of the map (30). The fixed points Y_{3i}^* of the map (36) correspond to the invariant circles associated with the period two fixed points for the map (30). For the map (30), the trivial fixed point $Y_0^{(1)}$ loses its stability upon crossing the half-line $L_1:\varepsilon_1=0$, $\varepsilon_{20}<0$, and period two fixed points bifurcate simultaneously from the trivial fixed point $Y_0^{(1)}$ via a period doubling bifurcation. On the line $L_2:\varepsilon_{20}=c_0\varepsilon_1/a$ $(\varepsilon_1<0)$, Hopf bifurcation associated with the fixed points $Y_1^{(2)}$and $Y_2^{(2)}$ occurs for the map (30), and two closed circles associated with the fixed points $Y_i^{(2)}$ exist in region R_4. Crossing the line $L_3:\varepsilon_{20}=d_0(a+c_0)\varepsilon_1/(ad_0+ab)$, $\varepsilon_1<0$, the invariant circles associated with the fixed points $Y_1^{(2)}$and $Y_2^{(2)}$ will change stability, and torus bifurcation occurs, which possibly lead to tori doubling, phase locked or quasi-attracting invariant circles. The trivial fixed point $Y_0^{(1)}$ loses its stability upon crossing the half-line $L_4:\varepsilon_{20}=0$, $(\varepsilon_1>0)$, and a closed circle bifurcates from the trivial fixed point $Y_0^{(1)}$ via a non-degenerate Hopf bifurcation. On the line $L_5:\varepsilon_{20}=d_0\varepsilon_1/b$ $(\varepsilon_{10}<0)$, the invariant circle associated with the trivial fixed point $Y_0^{(1)}$ will change its stability, and torus bifurcation occurs, which possibly lead to torus doubling, phase locking or quasi-attracting invariant circle. In region R_5, there exists possibly tori doubling, phasing locking or quasi-attracting invariant circle. A further investigation for bifurcation behavior of the normal form map (30), in region R_5, is necessary.

In the present case of scheme of coefficients of high order terms: $a>0$, $b>0$, $c_0<0$, $d_0<0$, $ad_0-bc_0<0$, $a+c_0>0$ and $b+d_0>0$, the bifurcation set for the map (36), near the critical point $\varepsilon=(\varepsilon_1,\varepsilon_{20})^{\mathrm{T}}=(0,0)^{\mathrm{T}}$, can be illustrated by Fig. 2. Only the positive (x,r) quadrant is shown in Fig. 2. Since the portraits are symmetric under reflection about r axis.

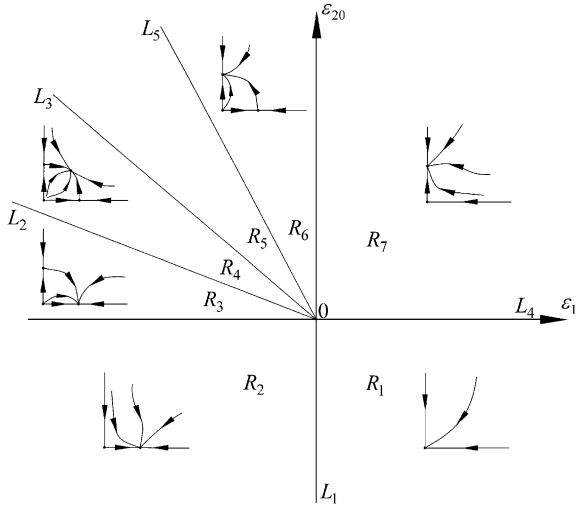

Fig. 2. The unfolding of simple case (I) $a>0$, $b>0$, $c_0<0$, $d_0<0$, $ad_0-bc_0<0$, $a+c_0>0$ and $b+d_0>0$. Bifurcation set of the map (36).

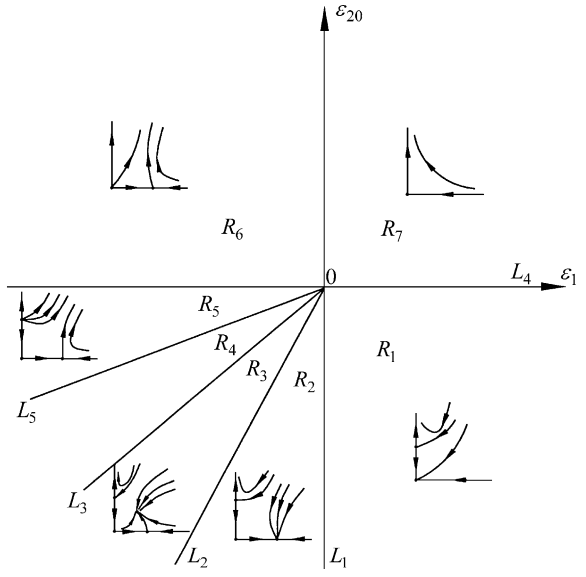

Fig. 3. The unfolding of simple case (II) $a>0$, $b>0$, $c_0>0$, $d_0>0$, $ad_0-bc_0<0$. Bifurcation set of the map (36).

The bounds of the regions shown in Fig. 2 can be listed as follows:

$$L_1=\{(\varepsilon_1,\varepsilon_{20}):\varepsilon_1=0,\varepsilon_{20}<0\};\quad L_2=\left\{(\varepsilon_1,\varepsilon_{20}):\varepsilon_{20}=\frac{c_0}{a}\varepsilon_1,\varepsilon_1<0\right\};$$

$$L_3=\left\{(\varepsilon_1,\varepsilon_{20}):\varepsilon_{20}=\frac{d_0(a+c_0)}{a(d_0+b)}\varepsilon_1,\varepsilon_1<0\right\};\quad L_4=\{(\varepsilon_1,\varepsilon_{20}):\varepsilon_{20}=0,\varepsilon_1>0\};$$

$$L_5=\left\{(\varepsilon_1,\varepsilon_{20}):\varepsilon_{20}=\frac{d_0}{b}\varepsilon_1,\varepsilon_1<0\right\}.$$

6.3. Simple case (II)

We analyze the unfolding of the simple case (II) associated with a scheme of coefficients of high order terms: $a>0$, $b>0$, $c_0>0$, $d_0>0$, $ad_0-bc_0<0$. The bifurcation set in the simple case is shown in Fig. 3. The formulae of the bounds L_1-L_5 of the regions, shown in Fig. 3, are the same algebraically as those in simple case (I).

Let us analyze the local behavior of the normal form map (30) near the bifurcation point $\varepsilon=(0,0,0)^{\mathrm{T}}$ by means of Fig. 3. By comparison with Fig. 2, we can find that period doubling bifurcation and further transition of the normal form map in the simple case (II) are similar to those in the simple case (I). However, the difference is that Hopf bifurcation of normal form map associated with the fixed point $Y_0^{(1)}$ in the simple case (I) is supercritical; in the simple case (II), subcritical. The difference of the unfolding of two simple cases can be observed obviously in the first and fourth quadrants of Figs. 2 and 3. In the sector region R_3, there exist six fixed points Y_0, Y_1^*, Y_{2i}^* and Y_{3i}^*. However, only the fixed points Y_{3i}^* are stable, and others unstable. By analyzing the Jacobian matrix of iterated map (37), we can obtain two real eigenvalues associated with the fixed points Y_{3i}^* in the sector region R_3, one of which escapes the unit circle from the point $(1,0)$ upon crossing the half-line L_3. The fixed points Y_{3i}^* are stable nodes in the region R_3, and not unstable in the sector region R_4. It is to be noted that very complicated behaviors occur in region R_4, i.e., there exists possibly tori doubling, phasing locking or quasi-attracting invariant circle for the normal form in the region.

6.4. Complex case

Now we continue to analyze the unfolding of the complex case associated with a scheme of coefficients of high order terms: $a<0$, $b<0$, $c_0<0$, $d_0<0$, $ad_0-bc_0<0$. The bifurcation set of map (36) in the complex case is shown in Fig. 4. In Fig. 4 only the positive (x,r) quadrant is shown. Since the portraits are symmetric under reflection about r axis. The bounds of the regions shown in Fig. 4 can be listed as follows:

$$L_1=\{(\varepsilon_1,\varepsilon_{20}):\varepsilon_1=0,\varepsilon_{20}<0\};\quad L_2=\{(\varepsilon_1,\varepsilon_{20}):\varepsilon_{20}=0,\varepsilon_1>0\};$$
$$L_3=\left\{(\varepsilon_1,\varepsilon_{20}):\varepsilon_{20}=\frac{d_0}{b}\varepsilon_1,\varepsilon_1>0\right\};\quad L_4=\left\{(\varepsilon_1,\varepsilon_{20}):\varepsilon_{20}=\frac{d_0(a+c_0)}{a(d_0+b)}\varepsilon_1,\varepsilon_1>0\right\};$$
$$L_5=\left\{(\varepsilon_1,\varepsilon_{20}):\varepsilon_{20}=\frac{c_0}{a}\varepsilon_1,\varepsilon_1>0\right\}.$$

By making a comparison between the map (36) and normal form map (30), we can unfold qualitative analyses for the normal form map in the complex case. Now we analyze the local behavior of the normal form map (30) near the bifurcation point $\varepsilon=(0,0,0)^{\mathrm{T}}$ by means of Fig. 4. For the normal form map, in region R_1 we have three fixed points, the stable trivial fixed point $Y_0^{(1)}=(0,0,0)^{\mathrm{T}}$ and unstable period two points

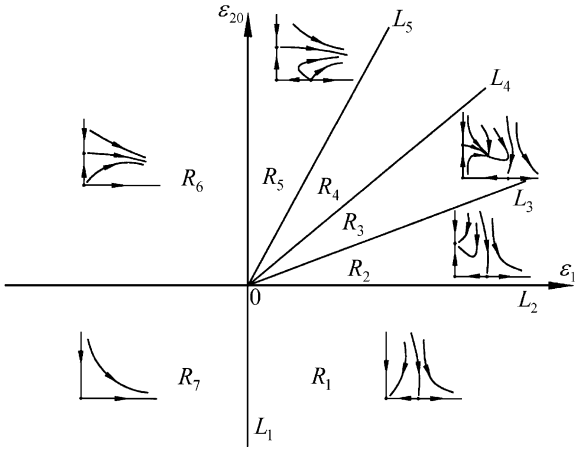

Fig. 4. The unfolding of a complex case, $a<0$, $b<0$, $c_0<0$, $d_0<0$, $ad_0-bc_0<0$. Bifurcation set of the map (36).

$Y^{(2)} = (Y_1^{(2)}, Y_2^{(2)})^{\mathrm{T}}$. As we have known, the trivial fixed point is node/focus, and period two points are saddles in the region R_1. As the parameters cross the line L_2 from the region R_1, Hopf bifurcation of the trivial fixed point $Y_0^{(1)}$ occurs so that a quasi-periodic attractor represented by the attracting closed circle is generated, and period two points retain their sense. As the parameters cross the line L_3 from the region R_2, the closed circle becomes non-attracting and the torus bifurcation occurs, which causes that the quasi-periodic attractor represented by two attracting closed circles is born. The quasi-periodic attractor represented by two closed circles is attracting in region R_3, and non-attracting in region R_4. In region R_5, there exist the unstable trivial fixed point, unstable periodic two points and non-attracting invariant circle associated with the trivial fixed point. In region R_6, we have the unstable trivial fixed point and non-attracting invariant circle.

It is to be noted that the quasi-periodic attractor represented by two closed circles is generated in different ways in the simple and complex cases. In the simple case, two closed circles are generated by Hopf bifurcation of period two points; in the complex case by torus bifurcation.

The bifurcation sets for the map (36), corresponding to the other cases of scheme of coefficients of high order terms, can be obtained by the similar method used in the above-mentioned three cases.

6.5. *Bifurcation set of the normal form map in simple case (I)*

In view of Jacobian matrices (33), we can find that there exist the period two fixed points $Y^{(2)} = (Y_1^{(2)}, Y_2^{(2)})^{\mathrm{T}}$ as $\varepsilon_1/a<0$. According to the unfolding of the simple case (I), the bifurcation set of the map (30), near $\varepsilon = (0,0,0)^{\mathrm{T}}$, can be further illustrated by Fig. 5 in which $\alpha<0$. Three possible cases for the eigenvalues λ_1 and $\lambda_{2,3}$ of Jacobian matrix Q_1 escaping the unit circle are shown in Fig. 6. The unfolding of normal form map (30), corresponding to the simple case (II) and complex case, can be obtained by the similar method used in the present case. The bounds of the regions shown in Fig. 5 can be listed as follows:

$$-\frac{e\varpi + c\alpha}{a}\varepsilon_1 + \alpha\varepsilon_2 + \varpi\varepsilon_3 = 0,$$

$$\begin{aligned} &L_{11}: \varepsilon_1 = 0,\ \ \varepsilon_2 > 0; \quad L_{12}: \varepsilon_2 = 0,\ \ \varepsilon_1 > 0; \quad L_{13}: \varepsilon_2 = \frac{e\varpi + c\alpha}{\alpha a}\varepsilon_1, \quad \varepsilon_1 < 0, \\ &L_{21}: \varepsilon_1 = 0,\ \ \varepsilon_3 < 0; \quad L_{22}: \varepsilon_3 = 0,\ \ \varepsilon_1 > 0; \quad L_{23}: \varepsilon_3 = \frac{e\varpi + c\alpha}{\varpi a}\varepsilon_1, \quad \varepsilon_1 < 0. \end{aligned} \tag{38}$$

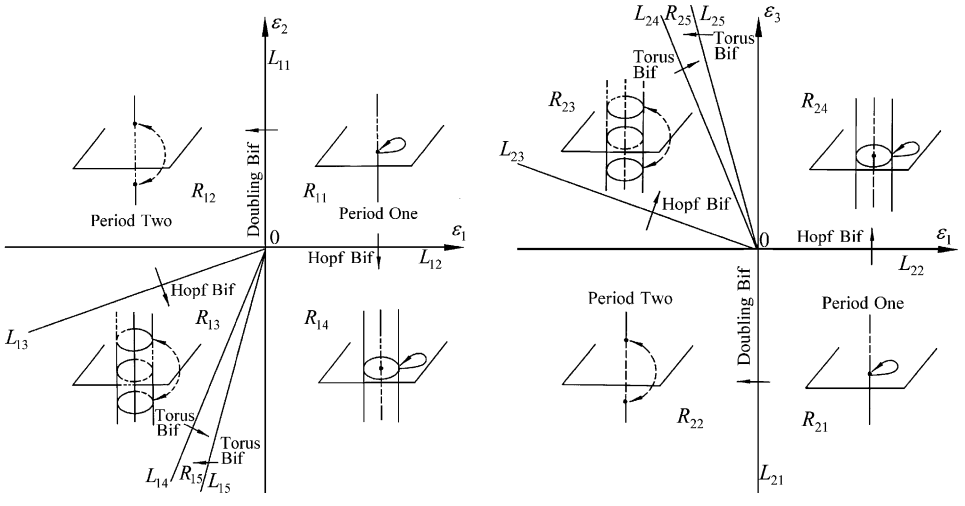

Fig. 5. Bifurcation set of the map (30) in the sample case (I).

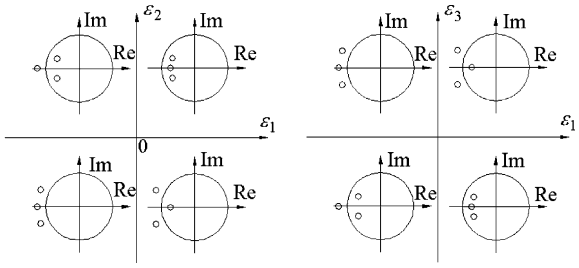

Fig. 6. Three possible cases for the eigenvalues λ_1 and $\lambda_{2,3}$ of Jacobian matrix Q_1, escaping the unit circle, in the sample case (I).

$$-\frac{\alpha d+\varpi f}{b}\varepsilon_1+\alpha\varepsilon_2=\varpi\varepsilon_3=0;\quad \frac{(\alpha d+\varpi f)(a+\alpha c+\varpi e)}{a(b+\alpha d+\varpi f)}\varepsilon_1+\alpha\varepsilon_2=\varpi\varepsilon_3=0,$$

$$L_{14}:\varepsilon_2=\frac{\alpha d+\varpi f}{\alpha b}\varepsilon_1,\quad \varepsilon_1<0;\quad L_{15}:\varepsilon_2=\frac{(\alpha d+\varpi f)(a+\alpha c+\varpi e)}{\alpha a(b+\alpha d+\varpi f)}\varepsilon_1,\quad \varepsilon_1<0,$$

$$L_{24}:\varepsilon_3=\frac{\alpha d+\varpi f}{\varpi b}\varepsilon_1,\quad \varepsilon_1<0;\quad L_{25}:\varepsilon_3=\frac{(\alpha d+\varpi f)(a+\alpha c+\varpi e)}{\varpi a(b+\alpha d+\varpi f)}\varepsilon_1,\quad \varepsilon_1<0. \tag{39}$$

Here we can assume, without loss of generality, $\alpha<0$. In the formulae (38) and (39), $e\varpi+c\alpha=c_0<0$, $\alpha d+\varpi f=d_0<0$.

By analyzing the eigenvalues of Jacobian matrices Q_1 and Q_2, we can conclude that when the parameters pass across the regions as $R_{i1}\to R_{i2}$ $(i=1,2)$, the type of the fixed point of period one changes from stable node to saddle; see Fig. 5. When the parameters cross the line L_{i1}, the period doubling bifurcation associated with the fixed point of period one occurs. When the parameters pass across the regions as $Ri_2\to Ri_3$, then the types of period two points $Y_1^{(2)}(Y_2^{(2)})$ change as stable node $\to$ stable focus $\to$ unstable focus. On the line L_{i3}, Hopf bifurcation of period two fixed points takes place. When the parameters pass across the regions as $R_{i1}\to R_{i4}$, the type of the fixed point of period one changes from stable focus to unstable focus, and on the line L_{i2}, Hopf bifurcation associated with the fixed point of period one occurs. The direction of Hopf bifurcation (supercritical or subcritical) depends on the high order terms of the normal form map.

By analysis of unfolding of the normal form map (30) in the present case, we can find that on the line L_{i4} the invariant circles associated with the fixed points of period two will change stability, and torus bifurcation occurs. On the line L_{i5} the invariant circle associated with the fixed point of period one will change stability, and torus bifurcation occurs.

According to the center manifold theory, we know that local behavior of the map $f(v,X)$, near the bifurcation point v_c, is equivalent to that of $\Phi(Y;\varepsilon)$ for ε near $\varepsilon=(0,0,0)^{\mathrm{T}}$. By virtue of the analyses of local bifurcation of normal form map (30), we can find out dynamical behavior of the map $f(v,X)$ in the case of codimension two bifurcation considered.

7. Numerical analyses

7.1. Codimension two bifurcation of a dual component system with vibro-impact

In this section, the analysis developed in the former section is verified by the presentation of results for the vibro-impact system shown in Fig. 1(a). The existence and stability of $q=1/1$ motion are analyzed explicitly. Also, local bifurcations at the points of change in stability, discussed in the previous section, are considered, thus giving some information on dynamical behavior near the point of codimension two bifurcation. The vibro-impact system, with system parameters $\mu_m=3.0$, $f_0=2.0$, $\delta=0.01$, $\zeta_1=\zeta_2=0.05$, $R=0.7$, has been chosen for analyzing the question. The forcing frequency ω and eigenfrequency ω_0 are taken as the control parameters, i.e. $v=(\omega_0,\omega)^{\mathrm{T}}$. The eigenvalues of $\mathrm{D}f(v,X^*)$ are computed with $\omega\in[3.138,3.32]$ and $\omega_0\in[1.26,1.35]$. All eigenvalues of $\mathrm{D}f(v,X^*)$ stay inside the unit circle for $v=(1.26,3.138)^{\mathrm{T}}$. By increasing ω and ω_0 gradually from the point $v=(1.26,3.138)^{\mathrm{T}}$ to change the control parameter v, we found that there

exist a real eigenvalue $\lambda_1(v_c) = -1.0000001$ and a pair of complex conjugate eigenvalues $\lambda_{2,3}(v_c) = -0.6305635 \pm 0.7761371\mathrm{i}$ ($|\lambda_{2,3}(v_c)| = 0.9999996$) which are very close to the unit circle, and the eigenvalue $\lambda_4(v)$ still stays inside the unit circle as v equals $v_c = (1.318563, 3.268051)^{\mathrm{T}}$. The eigenvalues $\lambda_1(v)$ and $\lambda_{2,3}(v)$ have already escaped the unit circle as ω and ω_0 pass through $\omega = 3.268052$ and $\omega_0 = 1.318565$ increasingly. The eigenvalues $\lambda_1(v)$ and $\lambda_{2,3}(v)$ almost escape the unit circle simultaneously, and $v_c = (1.318563, 3.268051)^{\mathrm{T}}$ may be approximately taken as the value of codimension two bifurcation.

Numerical analyses are carried out to unfold dynamic behavior of the impact system near the point of codimension two bifurcation. A local bifurcation portrait, near the value of bifurcation, is plotted in Fig. 7. The symbols (sub) and (sup) represent subcritical and supercritical, respectively, in the figure. The whole dynamical transitions from simulation are shown in the bifurcation diagrams for a series of values of ω_0 (Figs. 8 and 9) in which the velocities of the mass M_2, immediately after impact, are shown versus the forcing frequency ω. One can observe, from Figs. 8(a)–(c) that the system exhibits the stable $q = 1/1$ motion in two

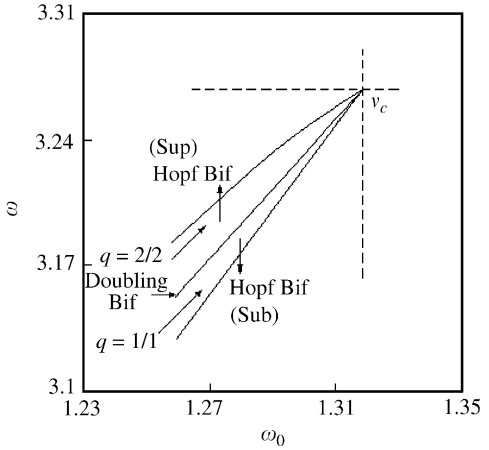

Fig. 7. Local bifurcation portrait near the point of condimension two bifurcation.

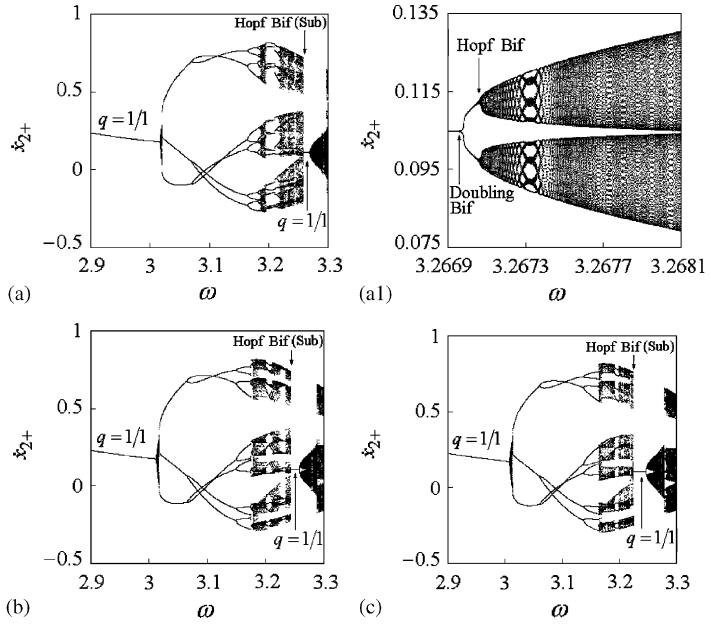

Fig. 8. Bifurcation diagrams near the point of codimension two bifurcation ($\omega_0 < 1.318563$): (a) $\omega_0 = 1.318$; (a1) $\omega_0 = 1.318$; (b) $\omega_0 = 1.31$; and (c) $\omega_0 = 1.305$.

different regions of forcing frequency, and the second one occurs near the value of codimension two bifurcation. The $q = 1/1$ motion, corresponding to the first region of ω, will undergo Hopf bifurcation with increasing ω. In the second region of forcing frequency associated with the $q = 1/1$ motion, the motion will undergo period doubling bifurcation with increase in the forcing frequency ω, and the $q = 2/2$ motion stabilizes. And then Hopf bifurcation of $q = 2/2$ motion occurs so that the quasi-periodic motion associated with the motion is generated. The transition processes of $q = 1/1$ motion are plotted locally in an amplified form in Fig. 8(a1). The results from simulation show that no period doubling cascade of $q = 1/1$ motion occurs, near the point of codimension two bifurcation, due to occurrence of Hopf bifurcation of $q = 2/2$ motion. Moreover, subcritical Hopf bifurcation of $q = 1/1$ motion, in the second window, occurs with decrease in the forcing frequency ω as seen in Figs. 7, 8 and 10. The type of $q = 1/1$ fixed point changes from stable focus to unstable focus. It should be noted that the second region of forcing frequency associated with $q = 1/1$ motion is narrow and vanishes for $\omega_0 > 1.318563$, and the $q = 1/1$ motion undergoes more complex bifurcation process than that in the first region; with decrease in the eigenfrequency ω_0 ($\omega_0 < 1.318563$), the second region of forcing frequency associated with $q = 1/1$ motion becomes wide gradually as seen in Fig. 7 and Figs. 8(a)–(c). The second window of $q = 1/1$ motion vanishes for $\omega_0 \geqslant 1.318563$; see Fig. 9. Some projected Poincaré sections are plotted in Figs. 10–12. The Poincaré section is taken in the form $\sigma = \{(x_1, \dot{x}_1, x_2, \dot{x}_2, \theta) \in \mathbf{R}^4 \times \mathbf{S},\ x_1 - x_2 = \delta,\ \dot{x}_1 = \dot{x}_{1+},\ \dot{x}_2 = \dot{x}_{2+}\}$, which is four-dimensional. The section is projected to the $(x_2, \dot{x}_{2+})$ or $(\tau, \dot{x}_{1+})$ plane, etc., which is called the projected Poincaré section. The $q = 1/1$ point, with the corresponding parameter v, is taken as the initial map point in every numerical analysis. We choose the eigenfrequency $\omega_0 = 1.318$ and change the forcing frequency ω in numerical analyses. It is shown, by the numerical results, that the system exhibits stable $q = 1/1$ impact motion with $\omega \in (3.266801, 3.266961)$. The $q = 1/1$ motion undergoes subcritical Hopf bifurcation as ω passes through $\omega_{c1} = 3.266801$ in a decreasing way, which is illustrated by the center manifold-normal form method of maps used in Ref. [23]. At

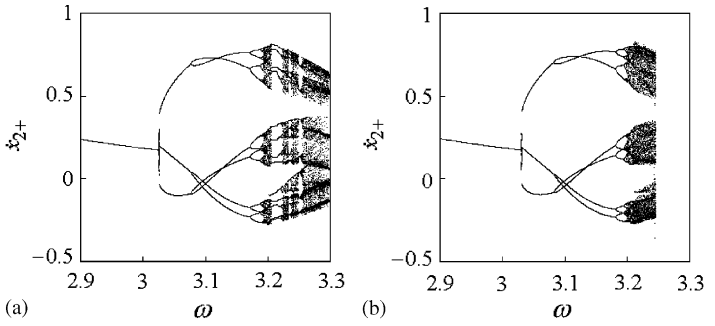

Fig. 9. Bifurcation diagrams near the point of codimension two bifurcation ($\omega_0 > 1.318563$): (a) $\omega_0 = 1.321$; and (b) $\omega_0 = 1.33$.

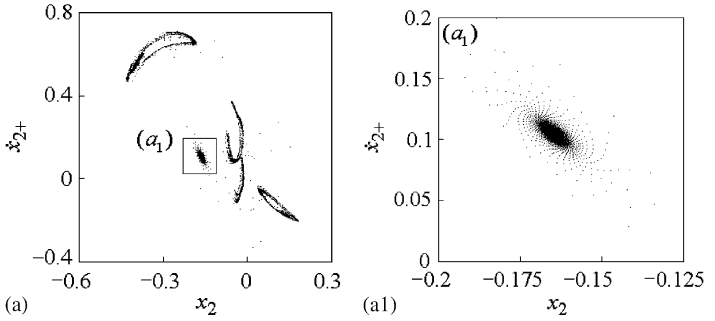

Fig. 10. The projected Poincaré sections: (a) transient points as well as chaotic attractor, starting from the initial condition near the $q = 1/1$ point (unstable focus), $\omega = 3.2667$, $\omega_0 = 1.318$; (a1) local map near the unstable $q = 1/1$ point, $\omega = 3.2667$, $\omega_0 = 1.318$.

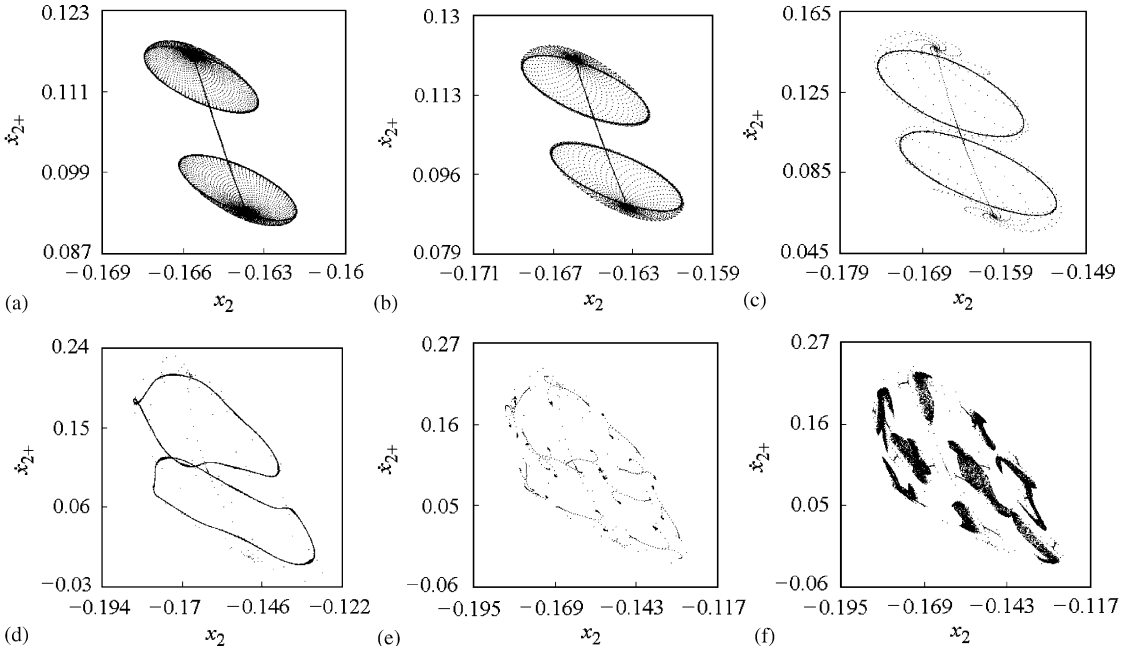

Fig. 11. The projected Poincaré sections: (a) transient points as well as the attracting invariant circles associated with $q = 2/2$ points, starting from the initial condition near the fixed point of $q = 1/1$ motion, $\omega = 3.2672$, $\omega_0 = 1.318$; (b) the attracting invariant circles associated with $q = 2/2$ points, $\omega = 3.2674$, $\omega_0 = 1.318$; (c) the attracting invariant circles associated with $q = 2/2$ points, $\omega = 3.27$, $\omega_0 = 1.318$; (d) the attracting invariant circles associated with $q = 2/2$ points, $\omega = 3.286$, $\omega_0 = 1.318$; (e) phase locking, $\omega = 3.287$, $\omega_0 = 1.318$; and (f) chaos, $\omega = 3.288$, $\omega_0 = 1.318$.

$\omega_{c1} = 3.266801$, the eigenvalues of $\mathrm{D}f(\omega, X^*)$ and associated bifurcation parameters are given as follows:

$$\lambda_{1,2}(\omega_{c1}) = -0.6306586 \pm 0.7760623\mathrm{i}, \quad \left|\lambda_{1,2}(\omega_{c1})\right| = 1.000001, \quad \lambda_3(\omega_{c1}) = -0.9980284,$$
$$\lambda_4(\omega_{c1}) = -0.314363, \quad \left.\frac{\mathrm{d}\left|\lambda_1(\mu)\right|}{\mathrm{d}\mu}\right|_{\mu=0} = 2.935115, \quad \mu = \omega_{c1} - \omega, \quad f_1(0) = -1.87756.$$

We can conclude, according to Refs. [23,47], that a subcritical Hopf bifurcation of $q = 1/1$ motion occurs for $\omega < 3.266801$, and the $q = 1/1$ fixed point changes from stable focus to unstable focus. Fig. 10 shows transient points as well as chaotic attractor, starting from initial condition near the unstable $q = 1/1$ focus for $\omega = 3.2667$.

Period doubling bifurcation of $q = 1/1$ motion occurs as ω is increased gradually and passes through $\omega_{c2} = 3.266961$, and the system exhibits stable $q = 2/2$ impact motion; see Fig. 8(a1). The $q = 2/2$ motion changes its stability for $\omega > 3.2671$, and Hopf bifurcation of $q = 2/2$ motion occurs so that the system exhibits quasi-periodic impact motion associated with $q = 2/2$ points. The quasi-periodic attractor is represented by two attracting invariant circles in projected Poincaré section. Figs. 11(a)–(d) show transient points as well as two attracting invariant circles, starting from the initial condition near the $q = 1/1$ point. It is to be noted that two attracting invariant circles are smooth in nature and symmetrical about the corresponding $q = 1/1$ point near the value $\omega = 3.2671$ of Hopf bifurcation of $q = 2/2$ motion. As the value of ω moves further away from the value of Hopf bifurcation, two attracting invariant circles expand, and the smoothness and symmetry of the quasi-periodic attractor are changed by degrees until they are destroyed. With further increase in ω, the phase locking takes place so that the quasi-periodic motion gets locked into a periodic attractor of higher (than period two) period (see Fig. 11(e)), which subsequently becomes unstable and chaotic; see Fig. 11(f).

The $q = 1/1$ motion, corresponding to the first region of ω, undergoes Hopf bifurcation as ω passes through $\omega_{c3} = 3.021382$ increasingly. With increase in ω, the quasi-periodic attractor gets locked into the $q = 3/3$ orbit,

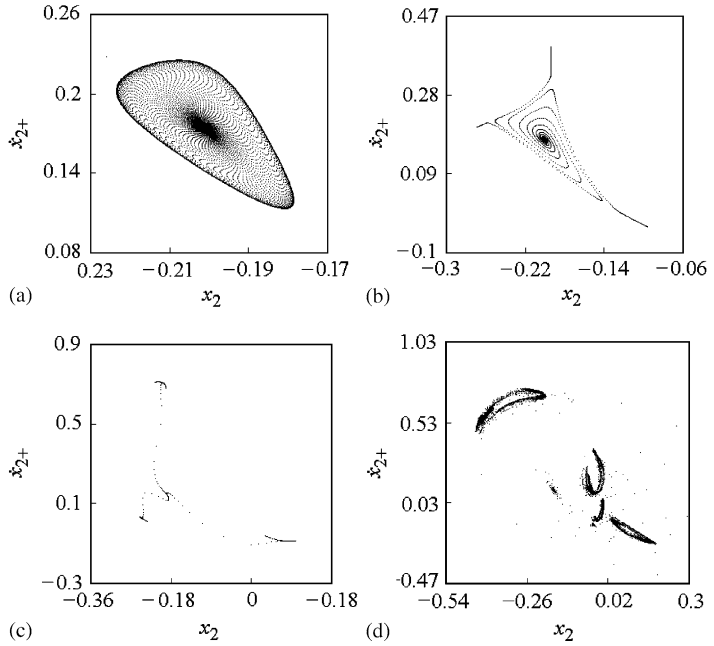

Fig. 12. The projected Poincaré sections: (a) the attracting invariant circle associated with $q = 1/1$ point, $\omega = 3.022$; (b) $q = 3/3$ fixed points, $\omega = 3.025$; (c) $q = 6/6$ fixed points, $\omega = 3.08$; and (d) chaos, $\omega = 3.25$.

and then period doubling bifurcation of $q = 3/3$ motion occurs, and the motion transits to chaos by Feigenbaum period-doubling cascade of $q = 3/3$ orbit; see Figs. 8 and 12.

7.2. Codimension two bifurcation of the impact-forming machinery

Two actual examples, the impact-forming machinery and inertial shaker, are chosen to further analyze the phenomenon of codimension two bifurcation of impact maps. The mechanical model for an impact-forming machinery with masses M_1 and M_2 is shown in Fig. 1(b) [48]. Displacements of the masses M_1 and M_2 are represented by X_1 and X_2, respectively. The masses are connected to linear springs with stiffnesses K_1, K_2 and K_3, and linear viscous dashpots with damping constants C_1, C_2 and C_3. The damping in the mechanical model is assumed as the proportional damping of the Rayleigh type. The excitation on mass M_2 is harmonic with amplitude $P = 2m_0r\Omega^2$. Ω is the excitation frequency, and τ is the phase angle. The mass M_1 impacts mutually with the mass M_2 when the difference of their displacements equals the gap Δ, i.e., $X_1(t)-X_2(t) = \Delta$. The impact is described by the conservation law of momentum and a coefficient of restitution R. Between consecutive impacts, the non-dimensional differential equations of motion are given by

$$\begin{bmatrix} \mu_m & 0 \\ 0 & 1 \end{bmatrix} \begin{Bmatrix} \ddot{x}_1 \\ \ddot{x}_2 \end{Bmatrix} + \begin{bmatrix} 2\zeta(1+\mu_{c_1}) & -2\zeta \\ -2\zeta & 2\zeta(1+\mu_{c_3}) \end{bmatrix} \begin{Bmatrix} \dot{x}_1 \\ \dot{x}_2 \end{Bmatrix} + \begin{bmatrix} \mu_{k_1}+1 & -1 \\ -1 & \mu_{k_3}+1 \end{bmatrix} \begin{Bmatrix} x_1 \\ x_2 \end{Bmatrix} = \begin{Bmatrix} 0 \\ 1 \end{Bmatrix} \sin(\omega t + \tau), \quad (40)$$

where a dot $(\cdot)$ denotes differentiation with to the non-dimensional time t, and the non-dimensional quantities

$$\mu_m = \frac{M_1}{M_2}, \quad \mu_{k_i} = \frac{K_i}{K_2}, \quad \mu_{c_i} = \frac{C_i}{C_2}, \quad i = 1, 3$$
$$\omega = \Omega\sqrt{\frac{M_2}{K_2}}, \quad t = T\sqrt{\frac{K_2}{M_2}}, \quad \zeta = \frac{C_2}{2\sqrt{K_2M_2}}, \quad \delta = \frac{\Delta \cdot K_2}{M_2 g}, \quad x_i = \frac{X_i K_2}{P} \quad (41)$$

have been introduced.

Let $\dot{x}_{i-}$ and $\dot{x}_{i+}$ $(i = 1, 2)$ represent the velocities of immediately before and after the impact of the masses M_i, respectively.

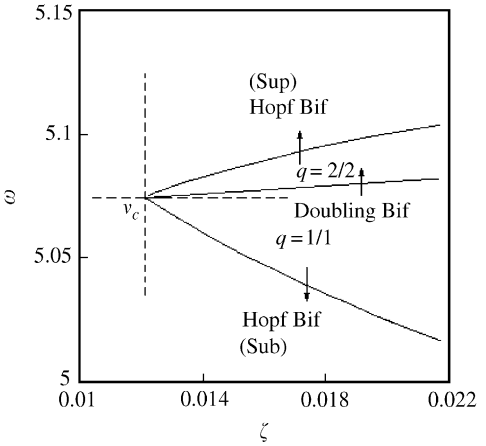

Fig. 13. Local bifurcation portrait near the point of codimension two bifurcation.

Let us choose a Poincaré section: $\sigma = \{(x_1, \dot{x}_1, x_2, \dot{x}_2, \theta) \in \mathbf{R}^4 \times \mathbf{S},\ x_1 - x_2 = \delta,\ \dot{x}_1 = \dot{x}_{1+},\ \dot{x}_2 = \dot{x}_{2+}\}$ to establish the Poincaré map $X' = f(v, X)$ [24].

The impact-forming system, with system parameters: $\mu_m = 2.0$, $\mu_{k_1} = 4.0$, $\mu_{k_3} = 3.0$, $\delta = 0.02$ and $R = 0.7$, has been chosen for analysis. The forcing frequency ω and damping ζ are taken as the control parameters, i.e. $v = (\zeta, \omega)^{\mathrm{T}}$. The eigenvalues of $\mathrm{D}f(v,\ X^*)$ are computed with $\omega \in [5.025, 5.2]$ and $\zeta \in [0.01, 0.02]$. All eigenvalues of $\mathrm{D}f(v,\ X^*)$ stay inside the unit circle for $v = (0.02, 5.025)^{\mathrm{T}}$. By gradually increasing ω and decreasing ζ from the point $v = (0.02, 5.025)^{\mathrm{T}}$ to change the control parameter v, we can obtain a real eigenvalue $\lambda_1(v_c) = -1.00000080$ and a pair of complex conjugate eigenvalues $\lambda_{2,3}(v_c) = -0.3768488 \pm 0.9262742\mathrm{i}$ ($|\lambda_{2,3}(v_c)| = 0.9999994$) which are very close to the unit circle, and the fourth eigenvalue ($\lambda_4(v_c) = -0.4031064$) still stays inside the unit circle as v equals $v_c = (0.0121275,\ 5.074519)^{\mathrm{T}}$. The eigenvalues $\lambda_1(v)$ and $\lambda_{2,3}(v)$ have escaped the unit circle as ω (increasingly) and ζ (decreasingly) pass through $\omega = 5.07452$ and $\zeta = 0.0121274$. The eigenvalues $\lambda_1(v)$ and $\lambda_{2,3}(v)$ almost escape the unit circle simultaneously, so $v_c = (0.0121275,\ 5.074519)^{\mathrm{T}}$ may be approximately taken as the value of codimension two bifurcation.

Local behavior of the impact-forming system, near the point of codimension two bifurcation, is obtained by numerical simulation. The local bifurcation portrait near the critical value is plotted in Fig. 13. The bifurcation diagrams are shown for a series of values of ζ in Fig. 14. There exist two windows of $q = 1/1$ motion in Figs. 14(a)–(c), the second of which occurs near the value of codimension two bifurcation. It should be noted that the second region of forcing frequency associated with $q = 1/1$ motion is narrow, and vanishes for $\zeta \leqslant 0.0121275$ (see Figs. 14(d) and (e)). With increase in damping ζ ($\zeta > 0.0121275$), the region of forcing frequency becomes wide generally; see Figs. 14(a)–(c). The $q = 1/1$ motion, corresponding to the first region of ω, will undergo supercritical Hopf bifurcation with increasing ω; see Fig. 14. In the second region of forcing frequency associated with the $q = 1/1$ motion, the motion will undergo period doubling bifurcation with increase in the forcing frequency ω, and the $q = 2/2$ motion stabilizes. And then Hopf bifurcation of $q = 2/2$ motion occurs so that the system exhibits the quasi-periodic motion associated with the motion. The transition process of $q = 1/1$ motion is plotted locally in an amplified form in Fig. 14(a1). The results from simulation show that no period doubling cascade of $q = 1/1$ motion occurs, near the point of codimension two bifurcation, due to occurrence of Hopf bifurcation of $q = 2/2$ motion. Moreover, subcritical Hopf bifurcation of $q = 1/1$ motion, in the second window, occurs with decrease in the forcing frequency ω as seen in Figs. 14(a)–(c) and Fig. 16, and the type of $q = 1/1$ fixed point changes from stable focus to unstable focus. Some projected Poincaré sections are plotted in Figs. 16–18. We choose the damping ratio $\zeta = 0.01225$ and change the forcing frequency ω in numerical analyses. The numerical results show that the system exhibits stable $q = 1/1$ motion with $\omega \in (5.073489,\ 5.074559)$ as seen in Figs. 14(a) and 15. The $q = 1/1$ motion undergoes subcritical Hopf bifurcation as ω passes through $\omega_{c1} = 5.073489$ decreasingly, and the type of $q = 1/1$ fixed point changes from stable focus to unstable focus; see Fig. 16. The period doubling bifurcation of $q = 1/1$ motion occurs as ω is increased gradually and passes through $\omega_{c2} = 5.074559$, and the system exhibits

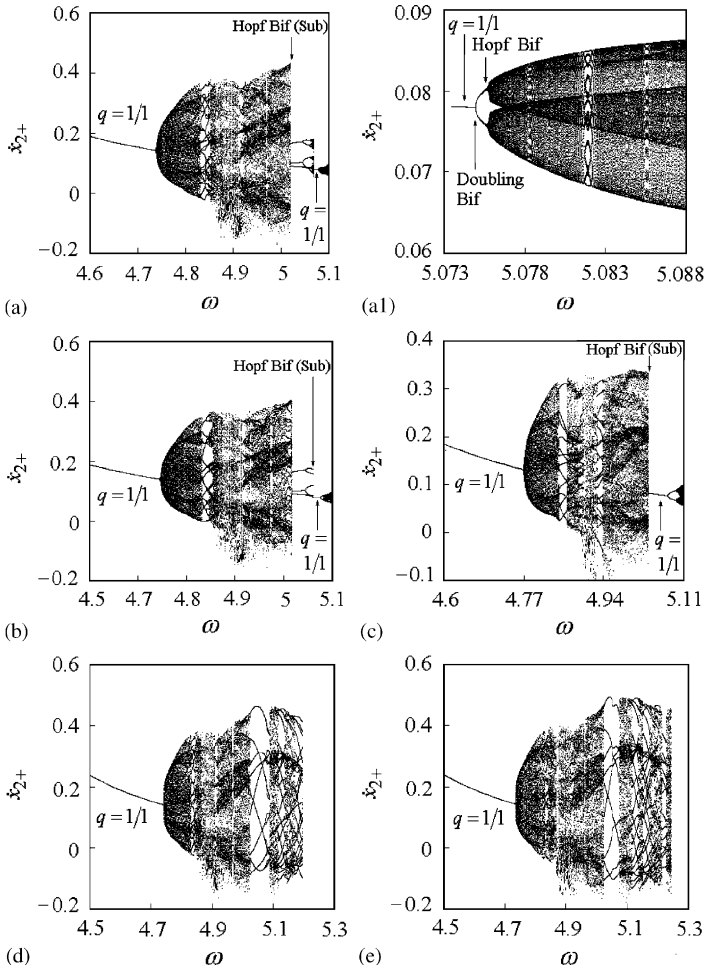

Fig. 14. Bifurcation diagrams near the point of codimension two bifurcation (a) $\zeta = 0.01225$; (a1) $\zeta = 0.01225$; (b) $\zeta = 0.0135$; (c) $\zeta = 0.0175$; (d) $\zeta = 0.012$; and (e) $\zeta = 0.007$.

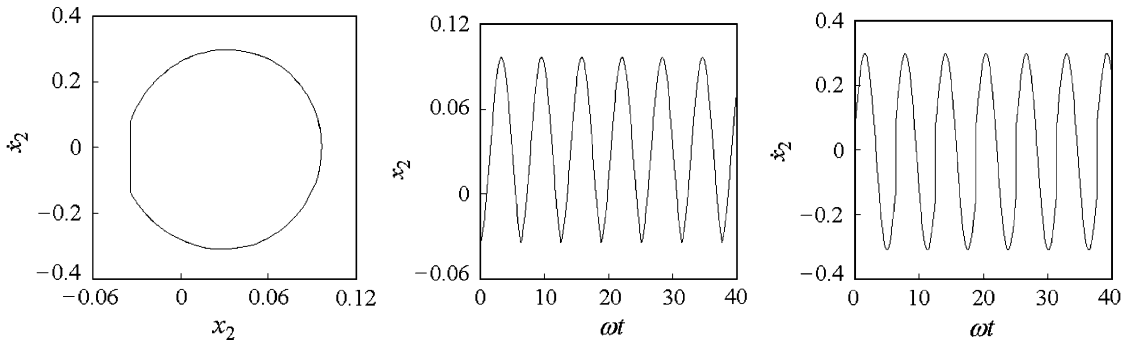

Fig. 15. The phase plane portrait and time trajectory of the mass M_2, $\omega = 5.074$, $\zeta = 0.01225$.

stable $q = 2/2$ motion; see Fig. 14(a1). The $q = 2/2$ motion changes its stability for $\omega > 5.07585$, and Hopf bifurcation of $q = 2/2$ motion occurs so that the system exhibits quasi-periodic impact motion associated with $q = 2/2$ points as seen in Figs. 17(a)–(d). With further increasing ω, the closed circle becomes quasi-attracting [23]. The quasi-attracting invariant circle is attracting for the map point inside the circle, and repelling for the

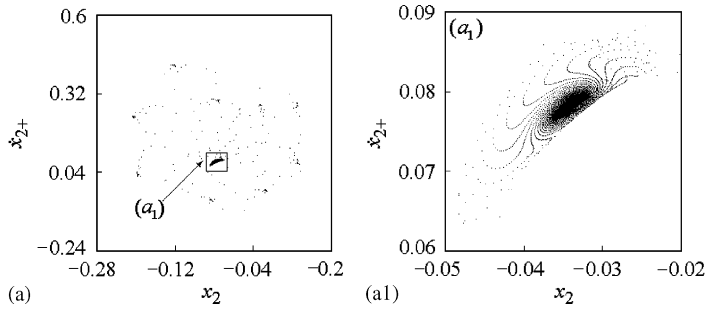

Fig. 16. The projected Poincaré sections: (a) transient points as well as $q = 9/9$ fixed points, starting from the initial codition near the $q = 1/1$ point (unstable focus), $\omega = 5.0724$, $\zeta = 0.01225$; and (a1) local map near the unstable $q = 1/1$ point, $\omega = 5.0724$, $\zeta = 0.01225$.

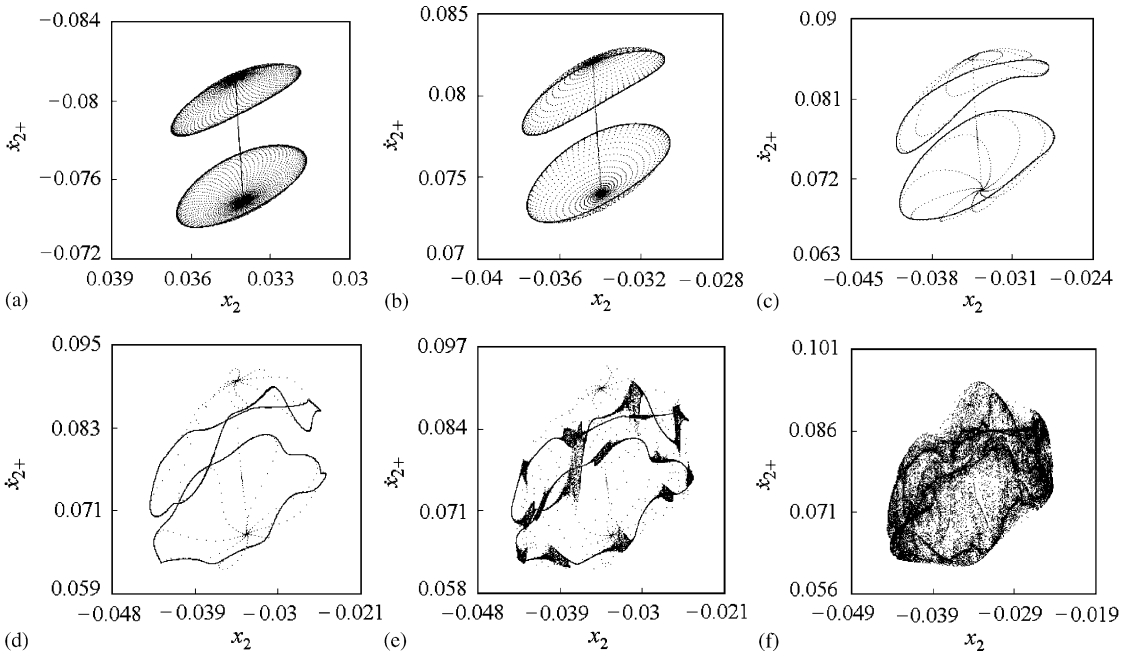

Fig. 17. The projected Poincaré sections: (a) transient points as well as the attracting invariant circles associated with $q = 2/2$ points, starting from the initial condition near the fixed point of $q = 1/1$ motion, $\omega = 5.076$, $\zeta = 0.01225$; (b) the attracting invariant circles associated with $q = 2/2$ points, $\omega = 5.077$, $\zeta = 0.01225$; (c) the attracting invariant circles associated with $q = 2/2$ points, $\omega = 5.083$, $\zeta = 0.01225$; (d) the attracting invariant circles associated with $q = 2/2$ points, $\omega = 5.093$, $\zeta = 0.01225$; (e) chaos, $\omega = 5.095$, $\zeta = 0.01225$; and (f) chaos, $\omega = 5.096$, $\zeta = 0.01225$.

map point outside it. The system falls into chaotic motion immediately via the quasi-attracting invariant circle; see Figs. 17(e) and (f).

The $q = 1/1$ motion, corresponding to the first region of ω, undergoes supercritical Hopf bifurcation as ω passes through $\omega_{c3} = 4.74017$ increasingly; see Figs. 14, 18(a) and (b). With increase in ω, the quasi-periodic attractor transits to chaos via phase locking; see Figs. 18(c) and (d).

7.3. Codimension two bifurcation of an inertial shaker

The inertial shaker is a typical vibro-impact machinery, which is widely used in casting industry. The mechanical model for an inertial vibro-impact shaker is shown in Fig. 1(c) [49]. The masses of shaker and cast are represented by M and m, respectively, and the displacements of them are represented by X_1 and X_2. The

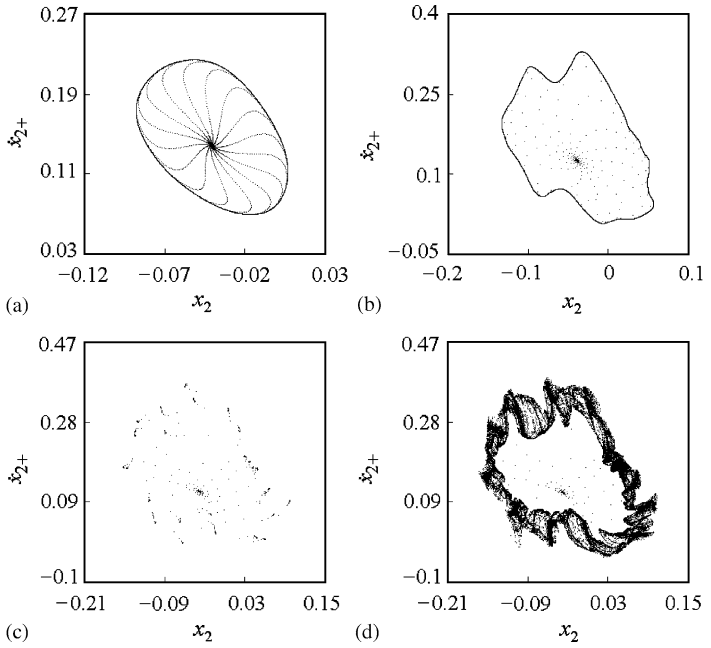

Fig. 18. The projected Poincaré sections: (a) transient points as well as the attracting invariant circles associated with $q = 1/1$ points, $\omega = 4.75$, $\zeta = 0.01225$; (b) the attracting invariant circles associated with $q = 1/1$ points, $\omega = 4.8$, $\zeta = 0.01225$; (c) phase locking $\omega = 4.85$, $\zeta = 0.01225$; and (d) chaos, $\omega = 4.855$, $\zeta = 0.01225$.

cast bounces on a flat horizontal surface of the shaker. The shaker is connected to the supporting base by the linear spring with stiffness K and dashpot with damping coefficient C. The excitation on the shaker is harmonic with amplitude F_0. The shaker impacts mutually with the cast when they are on the same height so that the cast exhibits the bouncing motion. The impact is described by a coefficient of restitution R. Between impacts, the non-dimensional differential equations of motion of the inertial shaker are given by

$$\ddot{x}_1 + 2\zeta\dot{x}_1 + x_1 = \sin(\omega t + \tau), \quad \ddot{x}_2 = -1/\beta. \tag{42}$$

Here the non-dimensional quantities are

$$\mu_m = \frac{m}{M}, \quad \omega = \Omega\sqrt{\frac{M}{K}}, \quad t = T\sqrt{\frac{K}{M}}, \quad \zeta = \frac{C}{2\sqrt{KM}}, \quad \beta = \frac{F_0}{Mg}, \quad x_i = \frac{X_i K}{F_0}. \tag{43}$$

Let $\dot{x}_{i-}$ and $\dot{x}_{i+}$ $(i = 1, 2)$ represent the velocities of immediately before and after the impact of two masses, respectively.

Let us choose a Poincaré section: $\sigma = \{(x_1, \dot{x}_1, x_2, \dot{x}_2, \theta) \in \mathbf{R}^4 \times \mathbf{S},\ x_1 - x_2 = 0,\ \dot{x}_1 = \dot{x}_{1+},\ \dot{x}_2 = \dot{x}_{2+}\}$ to establish the Poincaré map $X' = f(v, X)$ [24].

The inertial shaker, with system parameters $\zeta = 0.0788195$, $\beta = 2.2$ and $R = 0.7$, has been chosen for analyzing the question of codimension two bifurcation of periodic motion. The forcing frequency ω and distribution of masses μ_m are taken as the control parameters, i.e. $v = (\mu_m, \omega)^{\mathrm{T}}$. The eigenvalues of Jacobian matrix $\mathrm{D}f(v, X^*)$ are computed with $\omega \in [2.8, 2.934]$ and $\mu_m \in [0.45, 0.485]$. All eigenvalues of $\mathrm{D}f(v, X^*)$ stay inside the unit circle for $v = [0.485, 2.934]^{\mathrm{T}}$. By gradually decreasing ω and μ_m from the point $v = [0.485, 2.934]^{\mathrm{T}}$ to change the control parameter v, we found that there exist a real eigenvalue $\lambda_1(v_c) = -1.00000001$ and a pair of complex conjugate eigenvalues $\lambda_{2,3}(v_c) = -0.57579299 \pm 0.81759484\mathrm{i}$, $|\lambda_{2,3}(v_c)| = 0.99999944$ which are very close to the unit circle, and the eigenvalue $\lambda_4(v)$ still stays inside the unit circle $(\lambda_4(\omega_c) = -0.34619192)$ as v equals $v_c = (0.4621973, 2.85100014)^{\mathrm{T}}$. The eigenvalues $\lambda_1(v)$ and $\lambda_{2,3}(v)$ have already escaped the unit circle as ω and μ_m pass through $\omega = 2.85100012$ and $\mu_m = 0.46219715$ decreasingly. The eigenvalues $\lambda_1(v)$ and $\lambda_{2,3}(v)$ almost escape the unit circle simultaneously, and $v_c = (0.4621973, 2.85100014)^{\mathrm{T}}$ may be approximately taken as the value of codimension two bifurcation.

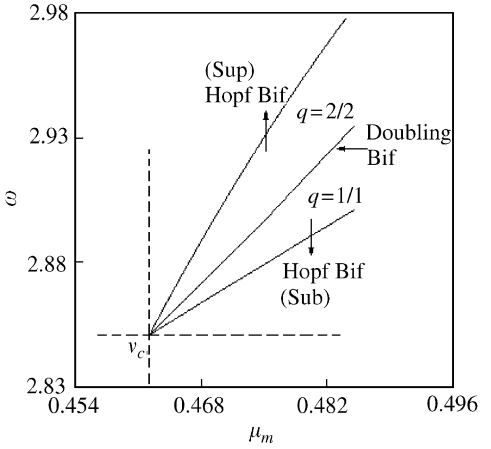

Fig. 19. Local bifurcation portrait near the point of codimension two bifurcation.

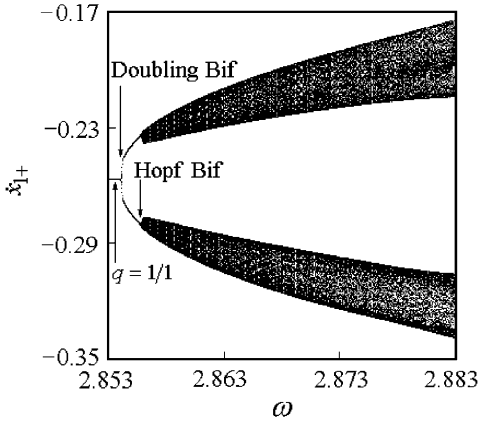

Fig. 20. Bifurcation diagram for $\mu_m = 0.4629$.

Local behavior of the inertial shaker, near the point of codimension two bifurcation, is obtained by numerical simulation, which is shown in Fig. 19 (see also Fig. 20).

Some projected Poincaré sections are plotted in Fig. 21. We choose the distribution of masses $\mu_m = 0.4629$ and change the forcing frequency ω in numerical analyses. It is shown, by numerical results, that the system exhibits stable $q = 1/1$ motion with $\omega \in (2.8525874, 2.853464)$. Period doubling bifurcation of $q = 1/1$ motion occurs as ω is increased gradually and passes through $\omega_{c1} = 2.853464$, and the system exhibits stable $q = 2/2$ impact motion. The $q = 2/2$ motion changes its stability for $\omega > 2.85443$, and Hopf bifurcation of $q = 2/2$ motion occurs so that the system exhibits quasi-periodic impact motion associated with $q = 2/2$ points as seen in Figs. 21(a)–(d). With further increase in ω, the phase locking takes place so that the quasi-periodic motion gets locked into a periodic attractor of higher (than period two) period, which subsequently becomes unstable and chaotic; see Figs. 21(e) and (f).

As ω passes through $\omega_{c2} = 2.8525874$ decreasingly, a subcritical Hopf bifurcation of $q = 1/1$ motion occurs. At the critical value $\omega_{c2} = 2.8525874$, the eigenvalues of Jacobian matrix $Df(\omega, X^*)$ and associated bifurcation parameters are given as follows:

$$\lambda_{1,2}(\omega_{c2}) = -0.57390452 \pm 0.81892223\mathrm{i}, \quad \left|\lambda_{1,2}(\omega_{c2})\right| = 1.00000001, \quad \lambda_3(\omega_{c2}) = -0.99753039,$$

$$\lambda_4(\omega_{c2}) = -0.3471157, \quad \left.\frac{\mathrm{d}\left|\lambda_{1,2}(\mu)\right|}{\mathrm{d}\mu}\right|_{\mu=0} = 5.611263, \quad \mu = \omega_{c2} - \omega, \quad f_1(0) = -2.7531,$$

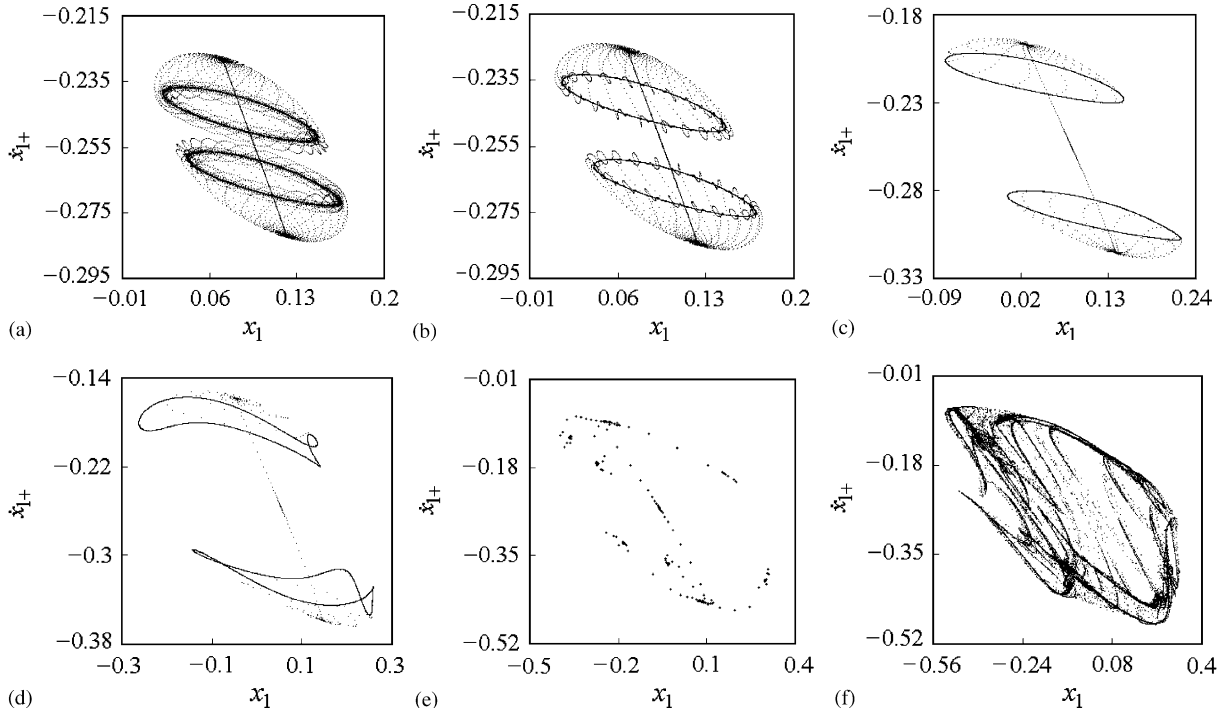

Fig. 21. The projected Poincaré sections: (a) transient points as well as the attracting invariant circles associated with $q = 2/2$ points, starting from the initial condition near the fixed point of $q = 1/1$ motion, $\omega = 2.856$, $\mu_m = 0.4629$; (b) the attracting invariant circles associated with $q = 2/2$ points, $\omega = 2.859$, $\mu_m = 0.4629$; (c) the attracting invariant circles associated with $q = 2/2$ points, $\omega = 2.85$, $\mu_m = 0.4629$; (d) the attracting invariant circles associated with $q = 2/2$ points, $\omega = 2.89$, $\mu_m = 0.4629$; (e) phase locking, $\omega = 2.97$, $\mu_m = 0.4629$; and (f) chaos, $\omega = 3$, $\mu_m = 0.4629$.

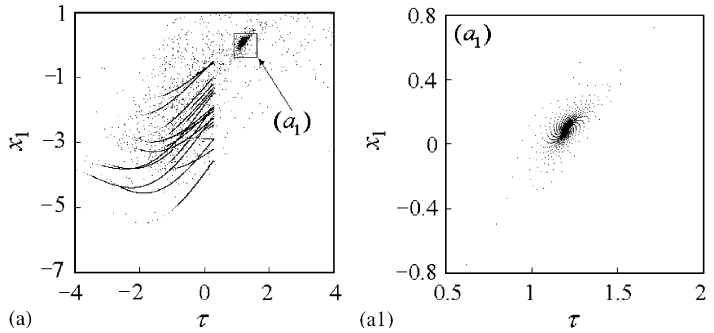

Fig. 22. The projected Poincaré sections: (a) transient points as well as chaotic attractor with chattering impacts, starting from the initial condition near the $q = 1/1$ point (unstable focus), $\omega = 2.851$, $\mu_m = 0.4629$; (a1) local map near the unstable $q = 1/1$ point, $\omega = 2.851$, $\mu_m = 0.4629$.

by which we know the Poincaré map of the vibro-impact system has a family of repelling invariant circles for $\omega > 2.8525874$, and the $q = 1/1$ point is stable. The fixed point of $q = 1/1$ impact motion becomes an unstable focus for $\omega < 2.8525874$, and transits to chaotic motion with chattering impacts; see Fig. 22. The chattering impacts mean that the time interval between any two consecutive impacts, in the motion, is far less than one cycle of the forcing [19]. The chattering impacts generally increase fretting of components of vibro-impact systems and noise levels.

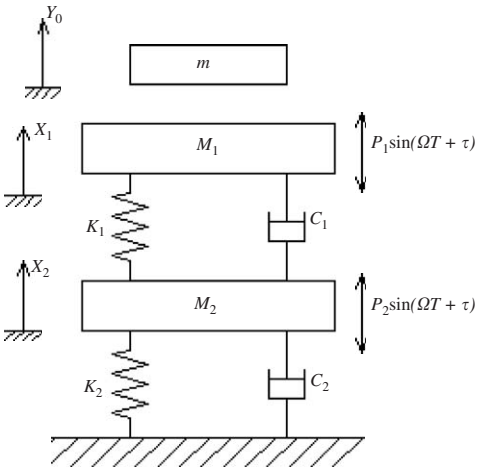

Fig. 23. Schematic of the vibro-impact system.

By studying codimension two bifurcation of three vibro-impact systems, we can find that these systems exhibit similar dynamical behavior near the points of codimension two bifurcations. It is to be noted that the three representative examples analyzed all correspond to the simple case (II) introduced in Section 6. A large number of numerical analyses for the three mechanical models of Fig. 1 have been done, but we have not found the other dynamical behaviors near the points of codimension two bifurcations except that in the simple case (II). However, we find the codimension two bifurcations and transition phenomena of periodic-impact motions associated the complex case by analyzing a three-degree-of-freedom vibro-bouncing system, which are introduced briefly in the following text.

7.4. Two examples associated with the complex case

In order to observe the codimension two bifurcations and transition phenomena of periodic-impact motions associated the complex case, we consider the mechanical model for a three-degree-of-freedom vibro-bouncing system, which is shown in Fig. 23. A body with mass m bounces on the flat horizontal surface of a two- degree-of-freedom vibro-bench with masses M_1 and M_2. Displacements of these masses m, M_1 and M_2 are represented by Y_0, X_1 and X_2, respectively. The masses M_1 and M_2 are connected to linear springs with stiffnesses K_1 and K_2, and linear viscous dashpots with damping constants C_1 and C_2. The excitations on both masses of the vibro-bench are harmonic with amplitudes P_1 and P_2. Ω is the excitation frequency, and τ is the phase angle. The mass M_1 impacts mutually with the bouncing mass m when they are on the same height, so the mass m exhibits the bouncing motion. The impact is described by the conservation law of momentum and a coefficient of restitution R, and it is assumed that the duration of impact is negligible compared to the period of the force.

The motion processes of the system, between any two consecutive impacts, are considered. Between any two consecutive impacts, the time T is always set to zero directly at the instant when the former impact is over, and the phase angle τ is used only to make a suitable choice for the origin of time in the calculation. The state of the vibro-impact system, immediately after impact, has become initial conditions in the subsequent process of the motion. Between consecutive impacts, the non-dimensional differential equations of motion are given by

$$\begin{bmatrix} 1 & 0 \\ 0 & \mu_m \end{bmatrix} \begin{Bmatrix} \ddot{x}_1 \\ \ddot{x}_2 \end{Bmatrix} + \begin{bmatrix} 2\zeta & -2\zeta \\ -2\zeta & 2\zeta(1+\mu_c) \end{bmatrix} \begin{Bmatrix} \dot{x}_1 \\ \dot{x}_2 \end{Bmatrix} + \begin{bmatrix} 1 & -1 \\ -1 & 1+\mu_k \end{bmatrix} \begin{Bmatrix} x_1 \\ x_2 \end{Bmatrix} = \begin{Bmatrix} 1-f_{20} \\ f_{20} \end{Bmatrix} \sin(\omega t+\tau), \tag{44}$$

$$\ddot{y} = -\beta. \tag{45}$$

where a dot $(\cdot)$ denotes differentiation with respect to the non-dimensional time t, and the non-dimensional quantities are given by

$$\mu_m = \frac{M_2}{M_1}, \quad \mu_k = \frac{K_2}{K_1}, \quad \mu_c = \frac{C_2}{C_1}, \quad f_{20} = \frac{P_2}{P_1 + P_2}, \quad \omega = \Omega\sqrt{\frac{M_1}{K_1}}, \quad t = T\sqrt{\frac{K_1}{M_1}},$$
$$\zeta = \frac{C_1}{2\sqrt{K_1 M_1}}, \quad x_i = \frac{X_i K_1}{P_1 + P_2}, \quad \beta = \frac{M_1 g}{P_1 + P_2}, \quad \mu = \frac{m}{M_1}, \quad y = \frac{Y_0 K_1}{P_1 + P_2}. \tag{46}$$

When the impact occurs, for $x_1(t) = y(t)$, the velocities of masses m and M_1 are changed according to the conservation law of momentum, and the impact equation of both masses m and M_1 and the coefficient of restitution R are given by

$$\dot{x}_{1-} + \mu\dot{y}_- = \dot{x}_{1+} + \mu\dot{y}_+, \quad \dot{x}_{1+} - \dot{y}_+ = -R(\dot{x}_{1-} - \dot{y}_-), \tag{47}$$

where the velocities of two masses M_1 and m, immediately before and after the impact, are represented respectively by $\dot{x}_{1-}$, $\dot{y}_-$, $\dot{x}_{1+}$ and $\dot{y}_+$.

The velocities, immediately after the impact, $\dot{x}_{1+}$ and $\dot{y}_+$ are given by

$$\dot{x}_{1+} = \frac{1 - \mu R}{1 + \mu}\dot{x}_{1-} + \frac{\mu(1 + R)}{1 + \mu}\dot{y}_-, \quad \dot{y}_+ = \frac{1 + R}{1 + \mu}\dot{x}_{1-} + \frac{\mu - R}{1 + \mu}\dot{y}_-. \tag{48}$$

Letting $\theta = \omega t$, we can choose a Poincaré section $\sigma = \{(x_1, \dot{x}_1, x_2, \dot{x}_2, y, \dot{y}, \theta) \in \mathbf{R}^6 \times \mathbf{S}, x_1 = y, \dot{x}_1 = \dot{x}_{1+}, \dot{y} = \dot{y}_+\}$ to establish Poincaré map of the impact system, which can be derived analytically by using the method introduced in Sections 2–4. The disturbed map of period one single-impact motion is expressed by

$$X' = \tilde{f}(v, X), \tag{49}$$

where $X \in \mathbf{R}^6$, v is varying parameter, and $v \in \mathbf{R}^1$ or $\mathbf{R}^2$; $X = X^* + \Delta X$, $X' = X^* + \Delta X'$, $\Delta X = (\Delta\dot{x}_{1+}, \Delta x_1, \Delta\dot{x}_2, \Delta x_2, \Delta\dot{y}_+, \Delta\tau)^{\mathrm{T}}$ and $\Delta X' = (\Delta\dot{x}'_{1+}, \Delta x'_1, \Delta\dot{x}'_2, \Delta x'_2, \Delta\dot{y}'_+, \Delta\tau')^{\mathrm{T}}$ are the disturbed vectors of X^*, $X^* = (\dot{x}_{1+}, x_{10}, \dot{x}_2, x_{20}, \dot{y}_+, \tau_0)^{\mathrm{T}}$ is a fixed point in the hyperplane σ.

An interesting torus doubling bifurcation is found to exist in the vibro-impact system near the point of codimension two bifurcation associated with the complex case. The torus doubling bifurcation makes the quasi-periodic attractor associated with $q = 1/1$ motion transit to the other quasi-periodic attractor represented by two attracting closed circles. The phenomena concerning torus doubling bifurcation are demonstrated by two examples given in the following text.

The vibro-impact system, with system parameters $\mu_m = 1.2$, $\mu_k = 1.5$, $\beta = 0.5$, $R = 0.7$, $f_{20} = 0$ and $\zeta = 0.05$, has been chosen for analysis. The forcing frequency ω and the distribution of masses μ are taken as the control parameters, i.e. $v = (\mu, \omega)^{\mathrm{T}}$. The eigenvalues of $\mathrm{D}\tilde{f}(v, X^*)$ are computed with $\omega \in [0.698, 0.72]$ and $\mu \in [0.629, 0.65]$. All eigenvalues of $\mathrm{D}\tilde{f}(v, X^*)$ stay inside the unit circle for $v = (0.715, 0.65)^{\mathrm{T}}$. By gradually decreasing μ and ω from the point $v = (0.715, 0.65)^{\mathrm{T}}$ to change the control parameters v, we obtain a real eigenvalue $\lambda_1(v_c) = -1.0000005$ and a pair of complex conjugate eigenvalues $\lambda_{2,3}(v_c) = 0.4301937 \pm 0.9027297\mathrm{i}$ $(|\lambda_{2,3}(v_c)| = 0.999994)$ which are very close to the unit circle, and the remaining eigenvalues still stay inside the unit circle $(\lambda_4(v_c) = -0.2114051, \ \lambda_{5,6}(v_c) = -0.03124346 \pm 0.3285842\mathrm{i})$ as v equals $v_c = (0.6998734, 0.6336134)^{\mathrm{T}}$. The eigenvalues $\lambda_1(v)$ and $\lambda_{2,3}(v)$ have escaped the unit circle as v passes through $v = (0.6998732, 0.6336132)^{\mathrm{T}}$ decreasingly. The eigenvalues $\lambda_1(v)$ and $\lambda_{2,3}(v)$ almost escape the unit circle simultaneously, so $v_c = (0.6998734, 0.6336134)^{\mathrm{T}}$ is approximately taken as the value of codimension two bifurcation.

Dynamical behavior of the system, near the point of codimension two bifurcation, is observed by numerical simulation. The partial bifurcation set near the critical value is plotted in Fig. 24(a). We choose the distribution of masses $\mu = 0.71$ and change the forcing frequency ω in numerical analyses. When ω passes through $\omega_{c1} = 0.6352363$ decreasingly, a complex conjugate pair eigenvalues of $\mathrm{D}\tilde{f}(\omega, X^*)$ escape the unit circle firstly, and Hopf bifurcation associated with $q = 1/1$ motion occurs. The quasi-periodic attractor is shown for $\omega = 0.635$ in Fig. 25(a). With decrease in the forcing frequency ω, instability of the closed circle associated with $q = 1/1$ point occurs, and torus bifurcation takes place so that two attracting invariant circles are generated; see Figs. 25(b) and (c) which show transient points, the non-attracting circle as well as the quasi-periodic attractor represented by two attracting invariant circles, starting from the initial condition near the

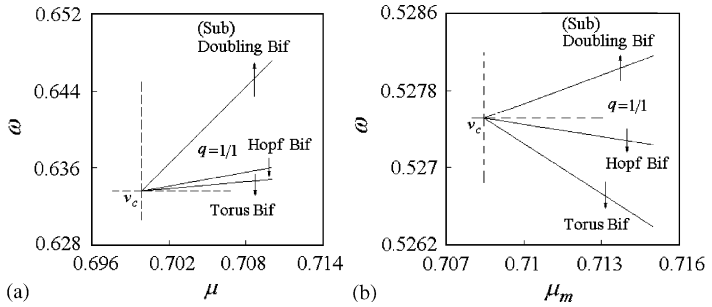

Fig. 24. The partial bifurcation set near the point of codimension two bifurcation: (a) system paramerers: $\mu_m = 1.2$, $\mu_k = 1.5$, $\beta = 0.5$, $R = 0.7$, $f_{20} = 0$ and $\zeta = 0.05$; and (b) system paramerers: $\mu = 0.3$, $\mu_k = 1$, $\mu_c = 1$, $\beta = 0.5$, $R = 0.6$, $f_{20} = 0$ and $\zeta = 0.05$.

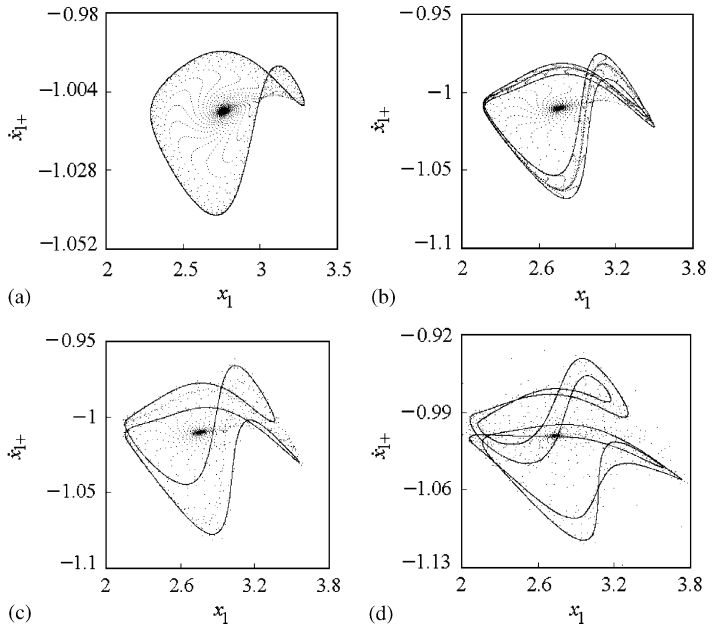

Fig. 25. The projected Poincaré sections: (a) transient points as well as the attracting invariant circle associated with $q = 1/1$ motion, starting from the initial condition near the fixed point of $q = 1/1$ motion, $\omega = 0.635$, $\mu = 0.71$; (b) transient points, the non-attracting invariant circle as well as two attracting invariant circles caused by torus bifurcation, starting from the initial condition near the fixed point of $q = 1/1$ motion, $\omega = 0.6348$, $\mu = 0.71$; (c) two attracting invariant circles, $\omega = 0.6347$, $\mu = 0.71$; (d) tori doubling, $\omega = 0.6342$, $\mu = 0.71$.

unstable $q = 1/1$ point. With further decrease in ω, two closed circles become quasi-attracting due to occurrence of chattering impacts [10,16]. The quasi-attracting invariant circles are attracting for the map point inside the circles, and repelling for the map point on or outside them. The system falls into chaotic motion immediately via the quasi-attracting invariant circles.

As the forcing frequency ω passes through $\omega_{c2} = 0.6471527$ increasingly, a real eigenvalue of Jacobian matrix $\mathrm{D}\tilde{f}(\omega, X^*)$ escape the unit circle from the point $(-1, 0)$, and period doubling bifurcation associated with $q = 1/1$ motion occurs. However, the period doubling bifurcation is subcritical. Stable $q = 1/1$ motion and unstable $q = 2/2$ motion coexist in the region $\omega \in (0.6352363, 0.6471527)$. As ω passes through $\omega_{c2} = 0.6471527$ increasingly, the $q = 1/1$ motion become unstable and there exists no $q = 2/2$ motion.

Another similar example is given by the system with system parameters: $\mu = 0.3$, $\mu_k = 1$, $\mu_c = 1$, $\beta = 0.5$, $f_{20} = 0$, $R = 0.6$ and $\zeta = 0.05$. The forcing frequency ω and distribution of masses μ_m are taken as the control parameters, i.e. $v = (\mu_m, \omega)^{\mathrm{T}}$. The eigenvalues of Jacobian matrix $\mathrm{D}\tilde{f}(v, X^*)$ are computed. All eigenvalues of

$D\tilde{f}(v, X^*)$ stay inside the unit circle for $v = (0.72, 0.5278)^T$. By gradually decreasing μ_m and ω from the point $v = (0.72, 0.5278)^T$ to change the control parameters v, we obtain the critical value $v_c = (0.7084388, 0.5275136)^T$, at which all eigenvalues of Jacobian matrix $D\tilde{f}(v, X^*)$ are given by

$$\lambda_{1,2}(v_c) = -0.28803001 \pm 0.95762230\mathrm{i}, \quad |\lambda_{1,2}(v_c)| = 1.0000, \quad \lambda_3(v_c) = -0.99999874,$$
$$\lambda_4(v_c) = -0.1849545, \quad \lambda_{5,6}(v_c) = -0.11229740 \pm 0.08878266\mathrm{i}.$$

The complex conjugate pair of eigenvalues $\lambda_{1,2}(v_c)$ and the real eigenvalue $\lambda_3(v_c)$ are very close to the unit circle. The eigenvalues $\lambda_{1,2}(v)$ and $\lambda_3(v)$ have escaped the unit circle as v passes through $v = (0.7084387,$

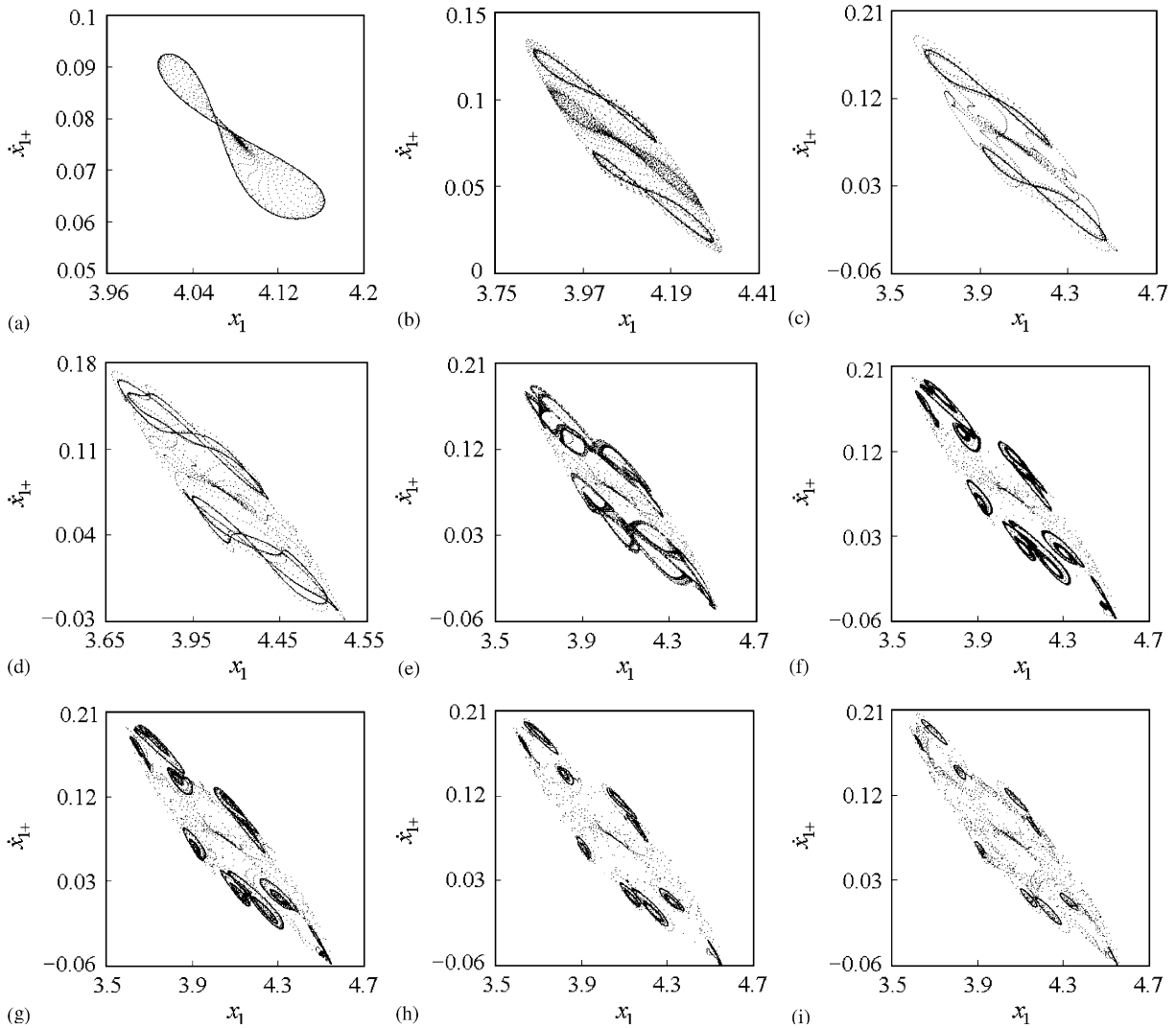

Fig. 26. The projected Poincaré sections: (a) transient points as well as the attracting invariant circle associated with $q = 1/1$ fixed point, starting from the initial condition near the fixed point of $q = 1/1$ motion, $\omega = 0.5275$, $\mu_m = 0.70845$; (b) transient points, the non-attracting invariant circle as well as two attracting invariant circles caused by torus bifurcation, starting from the initial condition near the fixed point of $q = 1/1$ motion, $\omega = 0.5274$, $\mu_m = 0.70845$; (c) two attracting invariant circles caused by torus bifurcation, $\omega = 0.5273$, $\mu_m = 0.70845$; (d) tori doubling, $\omega = 0.52723$, $\mu_m = 0.70845$; (e) chaos, $\omega = 0.52715$, $\mu_m = 0.70845$; (f) chaos, $\omega = 0.527085$, $\mu_m = 0.70845$; (g) chaos, $\omega = 0.52708$, $\mu_m = 0.70845$; (h) tori doubling associated with $q = 10/10$ fixed point, $\omega = 0.52706$, $\mu_m = 0.70845$; and (i) attracting invariant circles associated with $q = 10/10$ fixed point, $\omega = 0.52705$, $\mu_m = 0.70845$.

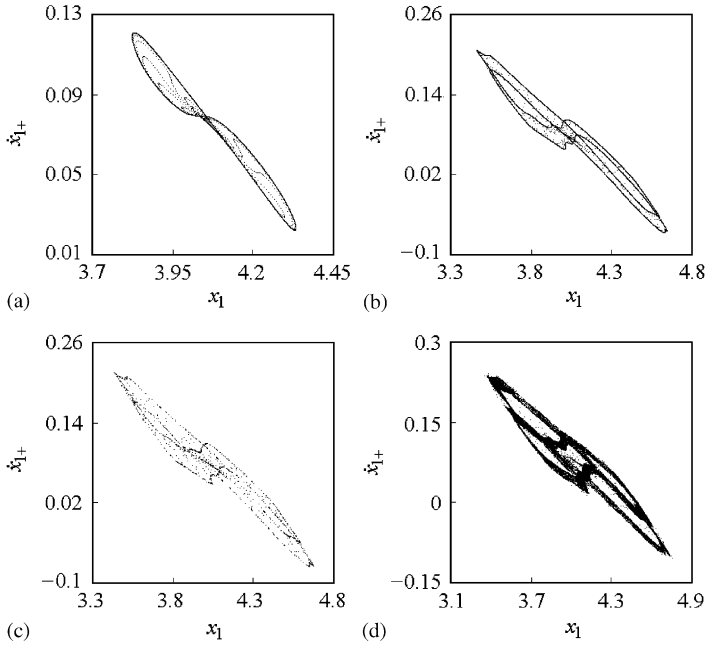

Fig. 27. The projected Poincaré sections: (a) transient points as well as the attracting invariant circle associated with $q = 1/1$ fixed point, starting from the initial condition near the fixed point of $q = 1/1$ motion, $\omega = 0.527$, $\mu_m = 0.715$; (b) transient points, the non-attracting invariant circle as well as two attracting invariant circles caused by torus bifurcation, starting from the initial condition near the fixed point of $q = 1/1$ motion, $\omega = 0.5264$, $\mu_m = 0.715$; (c) phase locking, $\omega = 0.52637$, $\mu_m = 0.715$; and (d) chaos, $\omega = 0.5263$, $\mu_m = 0.715$.

$0.5275134)^{\mathrm{T}}$ decreasingly. The eigenvalues $\lambda_{1,2}(v)$ and $\lambda_3(v)$ almost escape the unit circle simultaneously, so $v_c = (0.7084388, 0.5275136)^{\mathrm{T}}$ is approximately taken as the value of codimension two bifurcation.

The partial bifurcation set near the critical value is plotted in Fig. 24(b). Numerical results are shown for $\mu_m = 0.70845$, $\mu_m = 0.715$ and a series of values of ω in Figs. 26 and 27, respectively. The process of torus bifurcation can be observed clearly from the projected portraits of Poincaré map. The vibro-bouncing system with $\mu_m = 0.70845$ is analyzed firstly. The torus bifurcation and transition are shown for $\mu_m = 0.70845$ in Fig. 26. As the forcing frequency ω passes through the critical value $\omega_{c1} = 0.527511$ decreasingly, a complex conjugate pair eigenvalues of $\mathrm{D}\tilde{f}(\omega, X^*)$ escape the unit circle, and supercritical Hopf bifurcation associated with $q = 1/1$ motion occurs. The quasi-periodic attractor is shown for $\omega = 0.5275$ in Fig. 26(a). With decrease in ω, instability of the closed circle associated with $q = 1/1$ point occurs, and the torus bifurcation leads to two attracting invariant circles; see Figs. 26(b) and (c). With further decrease in ω, the two invariant circles become non-attracting and tori doubling are born, which subsequently becomes unstable and chaotic; see Figs. 26(d)–(g). And then the quasi-periodic attractors associated with $q = 10/10$ point are generated by degeneration of chaos, represented by ten tori doubling and ten closed circles in projected Poincaré sections, respectively; see Figs. 26(h) and (i).

The torus bifurcation and transition are shown for $\mu_m = 0.715$ in Fig. 27.

The dynamic behavior near the points of codimension two bifurcations, occurring in two examples of the system shown in Fig. 23, corresponds with the unfolding of a complex case shown in Fig. 4.

7.5. Symmetry of period two points and attracting invariant circles at the corresponding period one point

By analyzing local behavior of the normal form map near the point of codimension two bifurcation, we know that the period two points $Y^{(2)} = (Y_1^{(2)}, Y_2^{(2)})^{\mathrm{T}}$ are symmetrical about the origin. Moreover only the positive (x, r) quadrant is shown in Figs. 2–4, since the portraits are symmetric under reflection about r axis. The attracting invariant circles associated with $Y^{(2)} = (Y_1^{(2)}, Y_2^{(2)})^{\mathrm{T}}$ points are symmetrical about the origin near the critical value $\varepsilon = (0, 0, 0)^{\mathrm{T}}$. Because the type of $q = 2/2$ fixed points changes from node to focus and Hopf

bifurcation associated with $q = 2/2$ points occurs, no period doubling cascade emerges under the condiction of codimension two bifurcation. The $q = 2/2$ fixed points and closed tori associated with them are symmetrical about the corresponding $q = 1/1$ point near the value of codimension two bifurcation. We can observe the symmetry of $q = 2/2$ fixed points, about the corresponding $q = 1/1$ fixed point, as seen in the bifurcation diagrams (Figs. 8(a1), 14(a1) and 20). The results from simulation also show that the attracting invariant circles associated with $q = 2/2$ points are symmetrical about the corresponding $q = 1/1$ point near the value of Hopf bifurcation of $q = 2/2$ points; see bifurcation diagrams (Figs. 8(a1), 14(a1) and 20) and projected portraits of Poincaré map (Figs. 11(a)–(c), 17(a) and (b), 21(a)–(c)).

We can often observe a phenomenon in numerical analyses. As one of eigenvalues of Jacobian matrix $Df(\omega, X^*)$ escapes the unit circle of the complex plane from the point $(-1, 0)$ and a complex conjugate pair of eigenvalues are close to the unit circle but not very close to it, Hopf bifurcation associated with $q = 2/2$ points probably occurs. However, in this case the $q = 2/2$ fixed points and attracting invariant tori associated with them are generally non-symmetrical about the corresponding $q = 1/1$ point. This means that the symmetry of $q = 2/2$ fixed points and attracting invariant tori occurs only near the value of codimension two bifurcation. As the system parameters are far away from the critical parameters of codimension two bifurcation, no symmetry of $q = 2/2$ fixed points and attracting invariant tori exists. The asymmetrical $q = 2/2$ fixed points and attracting invariant tori can be observed in the following example.

Let us continue to consider the system shown in Fig. 1(a). The system, with system parameters $\mu_m = 0.8$, $f_0 = 2.0$, $\delta = 0.01$, $R = 0.8$, $\zeta_1 = \zeta_2 = 0.0$, $\omega_0 = 1.6$ and $n = 1$ is chosen for analysis. A real eigenvalue $\lambda_1(\omega)$ of $Df(\omega, X^*)$ escapes the unit circle from the point (–1, 0) with ω passing through $\omega_c = 2.470315$ increasingly, and the remainder of the spectrum of $Df(\omega, X^*)$ are strictly inside the unit circle, so period doubling bifurcation of $q = 1/1$ motion occurs. $\omega_c = 2.470315$ is the value of period doubling bifurcation, at which all eigenvalues of $Df(\omega, X^*)$ are

$$\lambda_1(\omega_c) = -1.000002, \quad \lambda_{2,3}(\omega_c) = 0.8189888 \pm 0.117085\mathrm{i}, \quad \lambda_4(\omega_c) = -0.9350552.$$

The results from simulation, by the bifurcation diagram and projected Poincaré sections, are epitomized in Figs. 28 and 29. The numerical results show that $q = 1/1$ motion stabilizes for $\omega \in [2.0, 2.470315]$. As ω passes though $\omega = 2.470315$, instability of $q = 1/1$ motion occurs, and $q = 2/2$ motion stabilizes. With changing the forcing frequency ω increasingly, $q = 2/2$ fixed points change from stable node to stable focus; see Figs. 29(a) and (b). And then instability of $q = 2/2$ points results in Hopf bifurcation associated with $q = 2/2$ fixed points. The quasi-periodic attractor associated with $q = 2/2$ points is shown for $\omega = 2.514$ and 2.517 in Figs. 29(c) and (d), respectively, which is represented by two closed circles in the projected Poincaré section. With further increase in ω, the phase locking takes place so that the quasi-periodic motion gets locked into a periodic attractor of higher (than period two) period (see Fig. 29(e)), which subsequently becomes unstable and chaotic; see Fig. 29(f). One can observe easily, from Figs. 28 and 29, that the $q = 2/2$ fixed points and attracting invariant tori associated with them are non-symmetrical about the corresponding $q = 1/1$ point.

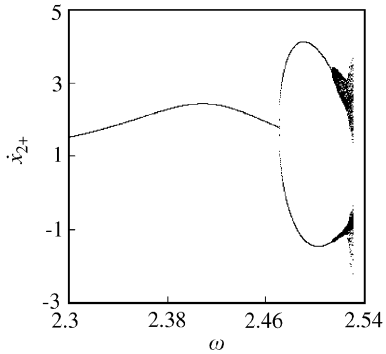

Fig. 28. Bifurcation diagram.

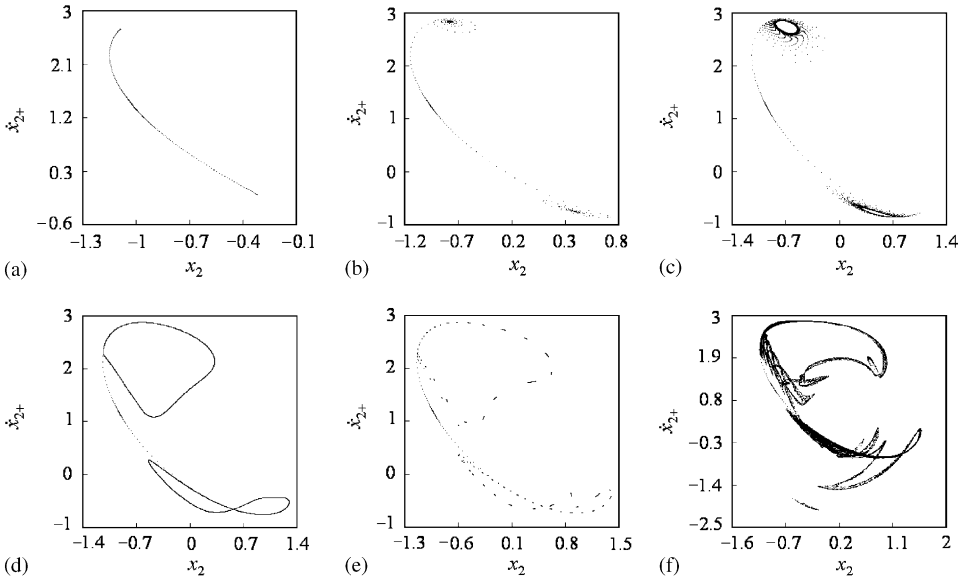

Fig. 29. The projected Poincaré sections: (a) transient points as well as $q = 2/2$ fixed points (node), starting from the initial condition near the fixed point of $q = 1/1$ motion, $\omega = 2.495$; (b) transient points as well as $q = 2/2$ fixed points (focus), starting from the initial condition near the fixed point of $q = 1/1$ motion, $\omega = 2.51$; (c) transient points as well as the attracting invariant circles associated with $q = 2/2$ points, starting from the initial condition near the fixed point of $q = 1/1$ motion, $\omega = 2.514$; (d) the attracting invariant circles associated with $q = 2/2$ points, $\omega = 2.517$; (e) phase locking, $\omega = 2.519$; and (f) chaos, $\omega = 2.525$.

8. Conclusions

Local codimension two bifurcation, involving a real eigenvalue and a complex conjugate pair escaping the unit circle simultaneously, is analyzed by using the center manifold theorem technique and normal forms for maps. Dynamical behavior of the vibro-impact systems, near the point of codimension two bifurcation, is investigated by qualitative analyses and numerical simulation. The vibro-impact system, under the condition of codimension two bifurcation, can exhibit more complicated quasi-periodic impact motions than those which occur in non-resonance, weak resonance [23] and strong resonance cases [24]. Near the point of codimension two bifurcation there exists not only Hopf bifurcation of $q = 1/1$ impact motion, but also Hopf bifurcation of $q = 2/2$ impact motion. The period doubling bifurcation of $q = 1/1$ motion is commonly existent near the point of codimension two bifurcation. However, no period doubling cascade of the motion emerges due to change of the type of $q = 2/2$ fixed points and occurrence of Hopf bifurcation of $q = 2/2$ motion. The types of $q = 2/2$ points usually change as stable node → stable focus → unstable focus with change of the control parameters. The $q = 2/2$ fixed points are symmetrical about the corresponding $q = 2/2$ point. The results from simulation show also that the attracting invariant circles associated with $q = 2/2$ points are smooth in nature and symmetrical about the corresponding $q = 1/1$ point near the value of Hopf bifurcation of $q = 2/2$ fixed points. As the value of ω moves further away from the value of Hopf bifurcation, two attracting invariant circles expand, and the smoothness and symmetry of the quasi-periodic attractor are changed by degrees until they are destroyed.

The strict condition of codimension two bifurcation is not easy to encounter in practical application of engineering. However, there exist the possibilities that actual nonlinear dynamical systems, with two varying parameters or more, work near the critical value of codimension two bifurcation due to change of parameters. The impact-forming machinery is a typical example. Besides the forcing frequency, ω, the gap varies also with different thicknesses of the formed workpieces [48]. Another representative example is the inertial vibro-impact shaker, where the distribution of masses is generally metabolic with casts of different masses, and the forcing frequency is also important parameter changed [49]. The change of multi-parameter possibly leads to the results that the vibro-impact systems work near the critical parameters of codimension two bifurcation. It

is necessary to study the bifurcations caused by change of multi-parameters and dynamical behavior of nonlinear systems near the points of bifurcations.

Acknowledgements

The authors gratefully acknowledge the support by National Natural Science Foundation (50475109, 10572055), Natural Science Foundation of Gansu Province Government of China (ZS-011-A25-010-Z, ZS-031-A25-007-Z (key item)) and 'Qing Lan' Talent Engineering by Lanzhou Jiaotong University.

Appendix A

A.1. The center manifold of high dimensional map under the condition of a codimension two bifurcation

Let us consider the map

$$X' = f(v, X), \tag{A.1}$$

in which, $f: \mathbf{R}^n \to \mathbf{R}^n$, $X \in \mathbf{R}^n$ $(n \geqslant 4)$, $v \in \mathbf{R}^2$. Let the map $f(v, X)$ be of class C^k $(k \geqslant 5)$, and assume that $X^*(v)$ is a fixed point for the map (A.1) for v in some neighborhood of a critical value $v = v_c$ at which the linearized map $\mathrm{D}f(v,\ X^*)$ satisfies the following assumption

H1. Jacobian matrix $\mathrm{D}f(v,\ X^*)$ has the eigenvalues $\lambda_1(v_c)$, $\lambda_2(v_c)$ and $\lambda_3(v_c)$ on the unit circle, in which $\lambda_1(v_c)$ is a real eigenvalue and $\lambda_{2,3}(v_c)$ are a pair of complex conjugate eigenvalues, and $\lambda_1(v_c) = -1$, $\lambda_2(v_c) = \bar{\lambda}_3(v_c)$, $|\lambda_{2,3}(v_c)| = 1$.

H2. The remainder of the spectrum of $\mathrm{D}f(v,\ X^*)$ are strictly inside the unit circle, i.e., $|\lambda_{2,3}(v_c)| < 1$, $i = 4, \ldots, n$.

Let $r_i(v)$ denote the eigenvector of $\mathrm{D}f(v,\ X^*)$ corresponding to the eigenvalue $\lambda_i(v)$ $(i = 1, 2, \ldots, n)$. If $\lambda_j(v)$ is one of a pair complex conjugate eigenvalues ($j \neq 1, 2, 3$, but j may be $4, \ldots, n-1$), the eigenmatrix may be expressed by $P = (r_1, \mathrm{Re}\ r_2, -\mathrm{Im}\ r_2, \ldots, \mathrm{Re}\ r_j, -\mathrm{Im}\ r_j, \ldots)$; If $\lambda_j(v)$ is a real eigenvalue ($j \neq 1, 2, 3$, but j may be $4, 5, \ldots, n$), then $P = (r_1, \mathrm{Re}\ r_2, -\mathrm{Im}\ r_2, \ldots, r_j, \ldots)$. For all v in some neighborhood of v_c, the map (A.1) under the change of variables

$$X = X^* + P\tilde{Y}, \quad v = v_c + \mu, \tag{A.2}$$

becomes

$$Y' = \tilde{F}(\mu,\ \tilde{Y}), \tag{A.3}$$

where $\mathrm{D}\tilde{F}(\mu, 0)$ has the form

$$\mathrm{D}\tilde{F}(\mu, 0) = \begin{bmatrix} \lambda_1 & 0 & 0 & 0 \\ 0 & \mathrm{Re}\ \lambda_2 & -\mathrm{Im}\ \lambda_2 & 0 \\ 0 & \mathrm{Im}\ \lambda_2 & \mathrm{Re}\ \lambda_2 & 0 \\ 0 & 0 & 0 & D_1 \end{bmatrix}, \tag{A.4}$$

in which $\lambda_1 = \tilde{\lambda}_1(\mu) = \lambda_1(v_c + \mu)$, $\lambda_2 = \tilde{\lambda}_2(\mu) = \lambda_2(v_c + \mu)$, $\tilde{\lambda}_1(0) = -1$, $\tilde{\lambda}_{2,3}(0) = \alpha \pm \mathrm{i}\varpi$. D_1 is a real matrix of degree $(n-3) \times (n-3)$ with eigenvalues $\tilde{\lambda}_4(\mu), \ldots, \tilde{\lambda}_{n-1}(\mu)$, $\tilde{\lambda}_n(\mu)$.

Let $z_1 = \tilde{y}_1$, $z_2 = \tilde{y}_2 + \mathrm{i}\tilde{y}_3$, $\bar{z}_2 = \tilde{y}_2 - \mathrm{i}\tilde{y}_3$, $z = (z_1, z_2, \bar{z}_2)^{\mathrm{T}}$, $G^{(1)} = F_1 - \lambda_1 z_1$, $G^{(2)} = F_2 + \mathrm{i}F_3 - \lambda_2 z_2$, $W = (\tilde{y}_4, \ldots, \tilde{y}_n)^{\mathrm{T}}$, $H = (\tilde{F}_4, \tilde{F}_5, \ldots, \tilde{F}_n)^{\mathrm{T}} - D_1 W$ and let us show that the map (A.3) may be written in the form

$$\begin{aligned} z_1' &= \lambda_1 z_1 + G^{(1)}(z_1, z_2, \bar{z}_2, W; \mu), \quad z_2' = \lambda_2 z_2 + G^{(2)}(z_1, z_2, \bar{z}_2, W; \mu), \\ W' &= D_1 W + H(z_1, z_2, \bar{z}_2, W; \mu). \end{aligned} \tag{A.5}$$

For the map (A.5), there exists a local center manifold [44,46], given by

$$\bar{W} = W(z_1, z_2, \bar{z}_2; \mu), \tag{A.6}$$

which satifies the condition $W(0,0,0;\mu) = W'_{z_1}(0,0,0;\mu) = W'_{z_2}(0,0,0;\mu) = W'_{\bar{z}_2}(0,0,0;\mu) = 0$.

On the center manifold the local behavior of the map (A.5) can be reduced, by substituting the formula (A.6) to the map (A.5), to a three-dimensional map. In order to determine the center manifold $W(z_1, z_2, \bar{z}_2; \mu)$, we have to expand $W(z_1, z_2, \bar{z}_2; \mu)$ in Tylor series about $(0,0,0,\mu)$ and solve the following equation:

$$W(z_1', z_2', \bar{z}_2'; \mu) = D_1 W(z_1, z_2, \bar{z}_2; \mu) + H(z_1, z_2, \bar{z}_2, W(z_1, z_2, \bar{z}_2; \mu); \mu). \tag{A.7}$$

The Tylor series of $W(z_1, z_2, \bar{z}_2; \mu)$ about $(0,0,0,\mu)$ is expressed by

$$W(z_1, z_2, \bar{z}_2; \mu) = \sum_{i+j+k=2}^{L} W_{ijk}(\mu) \frac{z_1^i z_2^j \bar{z}_2^k}{i!j!k!} + O(|z_1| + |z_2|)^{L+1}. \tag{A.8}$$

By substituting the formula (A.8) into Eq (A.7) and solving the equation for $W_{ijk}(\mu)$, we can obtain

$$\begin{aligned}
&W_{200} = (\lambda_1^2 - D_1)^{-1} H_{200}, \quad W_{020} = (\lambda_2^2 - D_1)^{-1} H_{020}, \quad W_{002} = (\bar{\lambda}_2^2 - D_1)^{-1} H_{002},\\
&W_{110} = (\lambda_1\lambda_2 - D_1)^{-1} H_{110}, \quad W_{011} = (\lambda_1\bar{\lambda}_2 - D_1)^{-1} H_{011}, \quad W_{101} = (\lambda_1\bar{\lambda}_2 - D_1)^{-1} H_{101},\\
&W_{300} = (\lambda_1^3 - D_1)^{-1}(H_{300} + 3H^1_{100} W_{200} - 3\lambda_1 G^{(1)}_{200} W_{200} - 3\lambda_1 W_{110} G^{(2)}_{200} - 3\lambda_1 W_{101} \bar{G}^{(2)}_{200}),\\
&W_{030} = (\lambda_2^3 - D_1)^{-1}(H_{030} + 3H^1_{010} W_{020} - 3\lambda_2 G^{(2)}_{020} W_{020} - 3\lambda_2 W_{011} \bar{G}^{(2)}_{200} - 3\lambda_2 W_{110} G^{(1)}_{020}),\\
&W_{003} = (\bar{\lambda}_2^3 - D_1)^{-1}(H_{003} + 3H^1_{001} W_{002} - 3\bar{\lambda}_2 G^{(1)}_{002} W_{101} - 3\bar{\lambda}_2 W_{011} G^{(2)}_{002} - 3\bar{\lambda}_2 W_{002} \bar{G}^{(2)}_{002}),\\
&W_{210} = (\lambda_1^2\lambda_2 - D_1)^{-1}(H_{210} + 2H^1_{100} W_{110} + H^1_{010} W_{200} - 2\lambda_1 G^{(1)}_{110} W_{200} - 2\lambda_1 W_{110} G^{(2)}_{110} - \lambda_2 W_{110} G^{(2)}_{200}\\
&\qquad - 2W_{101}\lambda_1 \bar{G}^{(2)}_{101} - W_{011}\lambda_2 \bar{G}^{(2)}_{200} - \lambda_2 W_{020} G^{(2)}_{200}),\\
&W_{201} = (\lambda_1^2\bar{\lambda}_2 - D_1)^{-1}(H_{201} + 2H^1_{100} W_{101} + H^1_{001} W_{200} - 2\lambda_1 G^{(1)}_{101} W_{200} - \bar{\lambda}_2 W_{002} \bar{G}^{(2)}_{200} - 2\lambda_1 W_{110} G^{(2)}_{101}\\
&\qquad - W_{011}\bar{\lambda}_2 G^{(2)}_{200} - 2W_{101}\lambda_1 \bar{G}^{(2)}_{110} - \bar{\lambda}_2 W_{101} G^{(1)}_{200}),\\
&W_{021} = (\lambda_2^2\bar{\lambda}_2 - D_1)^{-1}(H_{021} + 2H^1_{101} W_{011} + H^1_{001} W_{020} - \bar{\lambda}_2 \bar{G}^{(2)}_{002} W_{002} - 2\lambda_2 W_{020} G^{(2)}_{011} - \bar{\lambda}_2 W_{101} G^{(1)}_{020}\\
&\qquad - 2W_{011}\lambda_2 \bar{G}^{(2)}_{011} - W_{011}\bar{\lambda}_2 G^{(2)}_{020} - 2\lambda_2 W_{110} G^{(1)}_{011}),\\
&W_{102} = (\lambda_1^2\bar{\lambda}_2^2 - D_1)^{-1}(H_{102} + 2H^1_{001} W_{101} + H^1_{100} W_{002} - \lambda_1 G^{(1)}_{002} W_{200} - 2\bar{\lambda}_2 W_{002} \bar{G}^{(2)}_{110} - \lambda_1 W_{110} G^{(2)}_{002}\\
&\qquad - 2W_{011}\bar{\lambda}_2 G^{(2)}_{101} - W_{101}\lambda_1 \bar{G}^{(2)}_{020} - 2\bar{\lambda}_2 W_{101} G^{(1)}_{101}),\\
&W_{120} = (\lambda_1\lambda_2^2 - D_1)^{-1}(H_{120} + 2H^1_{010} W_{110} + H^1_{100} W_{020} - \lambda_1 G^{(1)}_{020} W_{200} - 2\lambda_2 G^{(2)}_{110} W_{020} - \lambda_1 W_{110} G^{(2)}_{020}\\
&\qquad - 2W_{110}\lambda_2 G^{(1)}_{110} - W_{101}\lambda_1 \bar{G}^{(2)}_{002} - 2\lambda_2 W_{011} \bar{G}^{(2)}_{101}),\\
&W_{111} = (\lambda_1\lambda_2\bar{\lambda}_2 - D_1)^{-1}(H_{111} + 2H^1_{010} W_{011} - \lambda_1 G^{(1)}_{011} W_{200} - \lambda_2 G^{(2)}_{101} W_{020} - \bar{\lambda}_2 \bar{G}^{(2)}_{101} W_{002} - \lambda_1 W_{110} G^{(2)}_{011}\\
&\qquad - W_{110}\lambda_2 G^{(1)}_{101} - \lambda_2 \bar{G}^{(2)}_{110} W_{011} - \bar{\lambda}_2 G^{(2)}_{110} W_{011} - W_{101}\lambda_1 \bar{G}^{(2)}_{011} - \bar{\lambda}_2 W_{101} G^{(1)}_{110}),
\end{aligned} \tag{A.9}$$

where W_{ijk}, $G^{(l)}_{ijk}$ and H_{ijk} denote $W_{ijk}(\mu)$, $G^{(l)}_{ijk}(\mu)$ and $H_{ijk}(\mu)$, respectively, and $G^{(l)}_{ijk}(\mu)$ and $H_{ijk}(\mu)$ are given by

$$G^{(l)}_{ijk} = \left.\frac{\partial^r G^{(l)}}{\partial z_1^i \partial z_2^j \partial \bar{z}_2^k}\right|_{(0,0,0,0;\mu)}, \quad H_{ijk} = \left.\frac{\partial^r H}{\partial z_1^i \partial z_2^j \partial \bar{z}_2^k}\right|_{(0,0,0,0;\mu)}, \quad r = i + j + k = 2, 3 \tag{A.10}$$

$$\begin{aligned}
&H^1_{100} = \frac{\partial}{\partial z_1}\left(\frac{\partial H}{\partial W_1}, \ldots, \frac{\partial H}{\partial W_{n-3}}\right)\Bigg|_{(0,0,0,0;\mu)}, \quad H^1_{010} = \frac{\partial}{\partial z_2}\left(\frac{\partial H}{\partial W_1}, \ldots, \frac{\partial H}{\partial W_{n-3}}\right)\Bigg|_{(0,0,0,0;\mu)},\\
&H^1_{001} = \frac{\partial}{\partial \bar{z}_2}\left(\frac{\partial H}{\partial W_1}, \ldots, \frac{\partial H}{\partial W_{n-3}}\right)\Bigg|_{(0,0,0,0;\mu)}.
\end{aligned} \tag{A.11}$$

Inserting the formulae (A.9) into the center manifold (A.8), we have

$$W(z_1, z_2, \bar{z}_2; \mu) = \sum_{i+j+k=2}^{3} W_{ijk}(\mu) \frac{z_1^i z_2^j \bar{z}_2^k}{i!j!k!} + \left(O(|z_1| + |z_2|)^4\right). \tag{A.12}$$

Let

$$z_1' = \lambda_1 z_1 + g^{(1)}(z_1, z_2, \bar{z}_2; \mu), \qquad z_2' = \lambda_2 z_2 + g^{(2)}(z_1, z_2, \bar{z}_2; \mu), \tag{A.13}$$

where

$$g^{(l)}(z_1, z_2, \bar{z}_2; \mu) = G^{(l)}(z_1, z_2, \bar{z}_2, W(z_1, z_2, \bar{z}_2; \mu); \mu). \tag{A.14}$$

The expanded form of $g^{(l)}(z_1, z_2, \bar{z}_2; \mu)$ is given by

$$g^{(l)}(z_1, z_2, \bar{z}_2; \mu) = \sum_{i+j+k=2}^{L} g_{ijk}^{(l)}(\mu) \frac{z_1^i z_2^j \bar{z}_2^k}{i!j!k!} + \left(O(|z_1| + |z_2|)^{L+1}\right), \quad (l = 1, 2). \tag{A.15}$$

Introducing the formulae (A.12) and (A.15) to the map (A.13), we obtain

$$\begin{aligned}
&g_{110}^{(l)} = G_{110}^{(l)},\ g_{011}^{(l)} = G_{011}^{(l)},\ g_{101}^{(l)} = G_{101}^{(l)},\ g_{200}^{(l)} = G_{200}^{(l)},\ g_{020}^{(l)} = G_{020}^{(l)},\ g_{002}^{(l)} = G_{002}^{(l)},\\
&g_{300}^{(l)} = G_{300}^{(l)} + 3G_{100}^{(l,1)} W_{200},\ g_{030}^{(l)} = G_{030}^{(l)} + 3G_{010}^{(l,1)} W_{020},\ g_{003}^{(l)} = G_{003}^{(l)} + 3G_{001}^{(l,1)} W_{002},\\
&g_{210}^{(l)} = G_{210}^{(l)} + 2G_{100}^{(l,1)} W_{110} + G_{011}^{(l,1)} W_{200},\ g_{120}^{(l)} = G_{120}^{(l)} + 2G_{010}^{(l,1)} W_{110} + G_{100}^{(l,1)} W_{020},\\
&g_{201}^{(l)} = G_{201}^{(l)} + 2G_{100}^{(l,1)} W_{101} + G_{001}^{(l,1)} W_{200},\ g_{102}^{(l)} = G_{102}^{(l)} + 2G_{001}^{(l,1)} W_{101} + G_{100}^{(l,1)} W_{002},\\
&g_{021}^{(l)} = G_{021}^{(l)} + 2G_{010}^{(l,1)} W_{011} + G_{001}^{(l,1)} W_{020},\ g_{012}^{(l)} = G_{012}^{(l)} + 2G_{001}^{(l,1)} W_{011} + G_{010}^{(l,1)} W_{002},\\
&g_{111}^{(l)} = G_{111}^{(l)} + 2G_{100}^{(l,1)} W_{011} + G_{010}^{(l,1)} W_{101} + G_{001}^{(l,1)} W_{110},
\end{aligned}$$

in which,

$$\begin{aligned}
&l = 1,\ 2, \quad G_{100}^{(l,1)} = \frac{\partial}{\partial z_1}\left(\frac{\partial G^{(l)}}{\partial W_1}, \ldots, \frac{\partial G^{(l)}}{\partial W_{n-3}}\right)\Big|_{(0,0,0,0;\mu)}, \quad G_{010}^{(l,1)} = \frac{\partial}{\partial z_2}\left(\frac{\partial G^{(l)}}{\partial W_1}, \ldots, \frac{\partial G^{(l)}}{\partial W_{n-3}}\right)\Big|_{(0,0,0,0;\mu)},\\
&G_{001}^{(l,1)} = \frac{\partial}{\partial \bar{z}_2}\left(\frac{\partial G}{\partial W_1}, \ldots, \frac{\partial G}{\partial W_{n-3}}\right)\Big|_{(0,0,0,0;\mu)}.
\end{aligned}$$

The map (A.1) has been reduced to a three-dimensional one by using a center manifold theorem technique. The three-dimensional map, in the complex form, is expressed by

$$\begin{aligned}
z_1' &= \tilde{\lambda}_1(\mu) z_1 + \sum_{i+j+k=2}^{3} g_{ijk}^{(1)}(\mu) \frac{z_1^i z_2^j \bar{z}_2^k}{i!j!k!} + O(|z_1| + |z_2|)^4,\\
z_2' &= \tilde{\lambda}_2(\mu) z_2 + \sum_{i+j+k=2}^{3} g_{ijk}^{(2)}(\mu) \frac{z_1^i z_2^j \bar{z}_2^k}{i!j!k!} + O(|z_1| + |z_2|)^4.
\end{aligned} \tag{A.16}$$

A.2. The normal form map

The three-dimensional map with two parameters is expressed briefly by

$$z' = F(\mu, z), \quad F(\mu, 0) = 0, \tag{A.17}$$

where $\mu = (\mu_1, \mu_2)^{\mathrm{T}}$, $z = (z_1, z_2, \bar{z}_2)^{\mathrm{T}}$, $z_1 = y_1, z_2 = y_2 + \mathrm{i}y_3$, $\bar{z}_2 = y_2 - \mathrm{i}y_3$.

Under the change of variables with parameters μ

$$z = G(\mu, Z) = Z + \Phi(\mu, Z), \quad \Phi(\mu, 0) = 0, \quad j \neq 1, 2, 3, \tag{A.18}$$

the three-dimensional map becomes the normal form

$$Z' = A_0 Z + N(\mu, Z), \quad N(\mu, 0) = 0, \tag{A.19}$$

in which $A_0 = \mathrm{Diag}[-1, \tilde{\lambda}_2(0), \bar{\tilde{\lambda}}_2(0)]$.

We can expand $F(\mu, z)$, $\Phi(\mu, Z)$ and $N(\mu, Z)$ as Taylor series in the variables μ, z, and Z, respectively, which are given by

$$F(\mu,z)=\sum_{p+q\geqslant 1}F_{pq}\left[\mu^{(p)},z^{(q)}\right],\quad \Phi(\mu,Z)=\sum_{p+q\geqslant 1}\Phi_{pq}\left[\mu^{(p)},Z^{(q)}\right],\quad N(\mu,Z)=\sum_{p+q\geqslant 1}N_{pq}\left[\mu^{(p)},Z^{(q)}\right], \tag{A.20}$$

where

$$F_{pq}=\frac{1}{p!q!}\cdot\frac{\partial^{p+q}F}{\partial\mu^p\partial z^q}(0,0),\quad \Phi_{pq}=\frac{1}{p!q!}\cdot\frac{\partial^{p+q}\Phi}{\partial\mu^p\partial Z^q}(0,0),\quad N_{pq}=\frac{1}{p!q!}\cdot\frac{\partial^{p+q}N}{\partial\mu^p\partial Z^q}(0,0).$$

By substituting the formula (A.20) into the map (A.18), we can obtain the equations

$$A_0\Phi_{11}[\mu,Z]-\Phi_{11}[\mu,A_0Z]=F_{11}[\mu,Z]-N_{11}[\mu,Z], \tag{A.21}$$

$$A_0\Phi_{02}\left[Z^{(2)}\right]-\Phi_{02}\left[(A_0Z)^{(2)}\right]=F_{02}\left[Z^{(2)}\right]-N_{02}\left[Z^{(2)}\right], \tag{A.22}$$

$$A_0\Phi_{03}\left[Z^{(3)}\right]-\Phi_{03}\left[(A_0Z)^{(3)}\right]=F_{03}\left[Z^{(3)}\right]+2\Phi_{02}\left[A_0Z,F_{02}\left[Z^{(2)}\right]\right]-N_{03}\left[Z^{(2)}\right]-2N_{02}\left[Z,\Phi_{02}\left[Z^{(2)}\right]\right], \tag{A.23}$$

$$A_0\Phi_{pq}\left[\mu^{(p)},Z^{(q)}\right]-\Phi_{pq}\left[\mu^{(p)},(A_0Z)^{(q)}\right]=R_{pq}\left[\mu^{(p)},Z^{(q)}\right]-N_{pq}\left[\mu^{(p)},Z^{(q)}\right],\ \ldots \tag{A.24}$$

The general form of Eqs. (A.21)–(A.24) is given by

$$B_q\Phi_{pq}=R_{pq}-N_{pq}, \tag{A.25}$$

where

$$B_q\Phi_{pq}\left[\mu^{(p)},Z^{(q)}\right]=A_0\Phi_{pq}\left[\mu^{(p)},Z^{(q)}\right]-\Phi_{pq}\left[\mu^{(p)},(A_0Z)^{(q)}\right]. \tag{A.26}$$

Let H_q represent the space of q order homogeneous polynomials, i.e. the elements of the space H_q consist of three-dimensional vectors, and component vector of every vector is a q order homogeneous expression associated with Z_1, Z_2 and $\bar{Z}_2$. Let B_q be a linear transformation in H_q. The space H_q may be expressed as the sum space of value subspace and complemented subspace. $R_{pq}-N_{pq}$ is reduced to value subspace of B_q by choosing the simpler form of N_{pq}, and Φ_{pq} is determined by using Eq. (A.25). Wherefore we can choose the basis for the space H_1

$$e_1=(Z_1,0,0)^{\mathrm{T}},\quad e_2=(Z_2,0,0)^{\mathrm{T}},\quad e_3=(\bar{Z}_2,0,0)^{\mathrm{T}},\quad \ldots\quad e_9=(0,0,\bar{Z}_2)^{\mathrm{T}}. \tag{A.27}$$

The images of e_i, on the matrix B_1, are

$$B_1e_1=0,\quad B_1e_2=(-1-\lambda)e_2,\quad B_1e_3=(-1-\bar{\lambda}),\quad B_1e_4=(\lambda+1)e_4,\quad B_1e_5=0,$$

$$B_1e_6=(\lambda-\bar{\lambda})e_6,\quad B_1e_7=(\bar{\lambda}+1)e_7,\quad B_1e_8=(\bar{\lambda}-\lambda)e_8,\quad B_1e_9=0,$$

where $\lambda=\lambda_2(0)=\alpha+\mathrm{i}\varpi$.

On the basis of (A.27), the matrix $\bar{B}_1$ may be expressed as

$$\bar{B}_1=\begin{bmatrix}0&0&0&0&0&0&0&0&0\\0&-1-\lambda&0&0&0&0&0&0&0\\0&0&-1-\bar{\lambda}&0&0&0&0&0&0\\0&0&0&\lambda+1&0&0&0&0&0\\0&0&0&0&0&0&0&0&0\\0&0&0&0&0&\lambda-\bar{\lambda}&0&0&0\\0&0&0&0&0&0&\bar{\lambda}+1&0&0\\0&0&0&0&0&0&0&\bar{\lambda}-\lambda&0\\0&0&0&0&0&0&0&0&0\end{bmatrix}.$$

Let the coordinates of Φ_{11}, N_{11} and F_{11} on the basis of $\{e_1,e_2,e_3,\ldots,e_9\}$ for H_1 be $\bar{\Phi}_{11}=\{\bar{\varphi}_1,\bar{\varphi}_2,\bar{\varphi}_3,\ldots,\bar{\varphi}_9\}^{\mathrm{T}}$, $\bar{N}_{11}=\{\bar{n}_1,\bar{n}_2,\bar{n}_3,\ldots,\bar{n}_9\}^{\mathrm{T}}$, $\bar{F}_{11}=\{\bar{f}_1,\bar{f}_2,\bar{f}_3,\ldots,\bar{f}_9\}^{\mathrm{T}}$.

The formula (A.21) can be represented by

$$\bar{B}_1\bar{\Phi}_{11} = \bar{F}_{11} - \bar{N}_{11}. \tag{A.28}$$

The solution for Eq. (A.28) is given by

$$\bar{\Phi}_{11} = \left\{ C_1, \frac{\bar{f}_2 - \bar{n}_2}{-1-\lambda}, \frac{\bar{f}_3 - \bar{n}_3}{-1-\bar{\lambda}}, \frac{\bar{f}_4 - \bar{n}_4}{\lambda+1}, C_2, \frac{\bar{f}_6 - \bar{n}_6}{\lambda-\bar{\lambda}}, \frac{\bar{f}_7 - \bar{n}_7}{\bar{\lambda}+1}, \frac{\bar{f}_8 - \bar{n}_8}{\bar{\lambda}-\lambda}, C_3 \right\},$$

$$\bar{N}_{11} = \{\bar{f}_1, 0, 0, 0, \bar{f}_5, 0, 0, 0, \bar{f}_9\}^{\mathrm{T}}, \tag{A.29}$$

in which C_1, C_2 and C_3 are arbitrary constants.

In the space H_2, we can choose the basis

$$e_1 = (Z_1^2, 0, 0)^{\mathrm{T}}, \quad e_2 = (Z_1 Z_2, 0, 0)^{\mathrm{T}}, \quad e_3 = (Z_1 \bar{Z}_2, 0, 0)^{\mathrm{T}}, \quad e_4 = (Z_2^2, 0, 0)^{\mathrm{T}},$$
$$e_5 = (Z_2 \bar{Z}_2, 0, 0)^{\mathrm{T}}, \quad e_6 = (\bar{Z}_2^2, 0, 0)^{\mathrm{T}}, \ldots, \quad e_{18} = (0, 0, \bar{Z}_2^2)^{\mathrm{T}},$$

on which, the matrix $\bar{B}_2$ is an invertible one, we can solve for the matrix form of the formula (A.22) by taking $N_{02}[Z^{(2)}] = 0$, which is given by

$$\bar{\Phi}_{02} = \bar{B}_2^{-1}\bar{F}_{02},$$

in which $\bar{\Phi}_{02}$ and $\bar{F}_{02}$ are the coordinate of $\Phi[Z^{(2)}]$ and $F_{02}[Z^{(2)}]$ on the basis of $\{e_i,\ i = 1, 2, \ldots, 18\}$ for H_2, respectively.

The basis of H_3 is taken by using the same method above-mentioned, and the basis for H_3 may be expressed by

$$e_1 = (Z_1^3, 0, 0)^{\mathrm{T}}, \quad e_2 = (Z_1^2 Z_2, 0, 0)^{\mathrm{T}}, \quad e_3 = (Z_1^2 \bar{Z}_2, 0, 0)^{\mathrm{T}}, \quad e_4 = (Z_1 Z_2^2, 0, 0)^{\mathrm{T}},$$
$$e_5 = (Z_1 \bar{Z}_2^2, 0, 0)^{\mathrm{T}}, \quad e_6 = (Z_1 Z_2 \bar{Z}_2, 0, 0)^{\mathrm{T}}, \quad e_7 = (Z_2^3, 0, 0)^{\mathrm{T}}, \quad e_8 = (Z_2^2 \bar{Z}_2, 0, 0)^{\mathrm{T}},$$
$$e_9 = (Z_2 \bar{Z}_2^2, 0, 0)^{\mathrm{T}}, \quad e_{10} = (\bar{Z}_2^3, 0, 0)^{\mathrm{T}}, \ \ldots, \ e_{30} = (0, 0, \bar{Z}_2^3)^{\mathrm{T}}.$$

The formula (A.23) may be expressed by

$$\bar{B}_3\bar{\Phi}_{03} = \bar{F}_{03} - \bar{N}_{03}. \tag{A.30}$$

The matrix $\bar{B}_3$ is a non-invertible one. $\bar{F}_{03}$, $\bar{\Phi}_{03}$ and $\bar{N}_{03}$ are the coordinates of $F_{03}[Z^{(3)}] + 2\Phi_{03}[A_0 Z, F_{02}[Z^{(2)}]]$, $\Phi_{03}[Z^{(3)}]$ and $N_{03}[Z^{(3)}]$ on the basis for H_3, respectively. $\bar{F}_{03} = (f_1, f_2, \ldots, f_{30})^{\mathrm{T}}$, $\bar{\Phi}_{03} = (\varphi_1, \varphi_2, \ldots, \varphi_{30})^{\mathrm{T}}$, $\bar{N}_{03} = (n_1, n_2, \ldots, n_{30})^{\mathrm{T}}$.

The solution for Eq. (A.30) is

$$\bar{\Phi}_{03} = \left\{ C_1, \frac{f_2 - n_2}{-1-\lambda}, \frac{f_3 - n_3}{-1-\bar{\lambda}}, \frac{f_4 - n_4}{-1+\lambda^2}, \frac{f_5 - n_5}{-1+\bar{\lambda}^2}, C_2, \frac{f_7 - n_7}{-1-\lambda^3}, \frac{f_8 - n_8}{-1-\lambda}, \ldots \frac{f_{30} - n_{30}}{\bar{\lambda} - \bar{\lambda}^3} \right\}, \tag{A.31}$$

$$\bar{N}_{03} = (f_1, 0, \ldots, 0, f_6, 0, \ldots 0, f_{12}, 0, \ldots 0, f_{18}, 0, \ldots 0, f_{23}, 0, \ldots, 0, f_{29}, 0), \tag{A.32}$$

in which, the symbol "…" denotes the term with zero value.

Let $\varepsilon_1 = \bar{f}_1$, $\tilde{\varepsilon}_2 = \bar{f}_5$ and $\tilde{\varepsilon}_3 = \bar{f}_9$ which are associated with the formula (A.29), $a = f_1$, $b = f_6$, $\tilde{c} = f_{12}$, $\tilde{d} = f_{18}$, $\tilde{e} = f_{23}$ and $\tilde{f} = f_{29}$ which are associated with the formula (A.32), and let us show that the simplest normal map $\Phi(Z; \tilde{\varepsilon})$, in the complex form, is given by

$$\begin{aligned}
Z_1' &= -Z_1 + \varepsilon_1 Z_1 + aZ_1^3 + bZ_1|Z_2|^2 + O\big((|Z_1| + |Z_2|)^5\big), \\
Z_2' &= \lambda_2(0)Z_2 + \tilde{\varepsilon}_2 Z_2 + \tilde{c}Z_1^2 Z_2 + \tilde{d}Z_2|Z_2|^2 + O\big((|Z_1| + |Z_2|)^5\big), \\
\bar{Z}'_2 &= \bar{\lambda}_2(0)\bar{Z}_2 + \tilde{\varepsilon}_3 \bar{Z}_2 + \tilde{e}Z_1^2 \bar{Z}_2 + \tilde{f}\bar{Z}_2|Z_2|^2 + O\big((|Z_1| + |Z_2|)^5\big),
\end{aligned} \tag{A.33}$$

where $Z = (Z_1, Z_2, \bar{Z}_2)^{\mathrm{T}}$, $\varepsilon = (\varepsilon_1, \tilde{\varepsilon}_2, \tilde{\varepsilon}_3)^{\mathrm{T}}$, $\tilde{\varepsilon}_i = \tilde{\varepsilon}_i(\mu)$, $\tilde{\varepsilon}_i(0) = 0$, $i = 1, 2, 3$.

The normal form map $\Phi(Y;\varepsilon)$, in the real form, is given by

$$\begin{aligned} y_1' &= -y_1 + \varepsilon_1 y_1 + a y_1^3 + b y_1(y_2^2 + y_3^2) + \text{h.o.t}, \\ y_2' &= (\alpha + \varepsilon_2) y_2 - (\varpi + \varepsilon_3) y_3 + (c y_2 - e y_3) y_1^2 + (d y_2 - f y_3)(y_2^2 + y_3^2) + \text{h.o.t}, \\ y_3' &= (\varpi + \varepsilon_3) y_2 + (\alpha + \varepsilon_2) y_3 + (c y_3 + e y_2) y_1^2 + (d y_3 + f y_2)(y_2^2 + y_3^2) + \text{h.o.t}, \end{aligned} \tag{A.34}$$

where $Y = (y_1, y_2, y_3)^{\mathrm{T}}$, $\varepsilon = (\varepsilon_1, \varepsilon_2, \varepsilon_3)^{\mathrm{T}}$, $\varepsilon_i = \varepsilon_i(\mu)$, $\varepsilon_i(0) = 0$, $i = 1, 2, 3$.

References

[1] P.J. Holmes, The dynamics of repeated impacts with a sinusoidally vibrating table, *Journal of Sound and Vibration* 84 (2) (1982) 173–189.

[2] S.W. Shaw, P.J. Holmes, A periodically forced piecewise linear oscillator, *Journal of Sound and Vibration* 90 (1) (1983) 129–155.

[3] S.W. Shaw, The dynamics of a harmonically excited system having rigid amplitude constraints Part 2: Chaotic motions and global bifurcations, *Journal of Applied Mechanics* 52 (1985) 459–464.

[4] G.S. Whiston, Global dynamics of vibro-impacting linear oscillator, *Journal of Sound and Vibration* 118 (3) (1987) 395–429.

[5] K.M. Cone, R.I. Zadoks, A numerical study of an impact oscillator with the addition of dry friction, *Journal of Sound & Vibration* 188 (5) (1995) 659–683.

[6] C.S. Yim, Huan Lin, Nonlinear impact and chaotic response of slender rocking objects, *Journal of Engineering. Mechanics* 117 (9) (1991) 2079–2100.

[7] F. Peterka, Comments on "Periodic and chaotic behaviour of a threshold-limited two-degree-of-freedom system", *Journal of Sound and Vibration* 165 (2) (1993) 369–372.

[8] J.O. Aidanp ää, B.R. Gupta, Periodic and chaotic behaviour of a threshold-limited two-degree-of-freedom system, *Journal of Sound and Vibration* 165 (2) (1993) 305–327.

[9] A.B. Nordmark, Non-periodic motion caused by grazing incidence in an impact oscillator, *Journal of Sound and Vibration* 145 (2) (1991) 279–297.

[10] G.S. Whiston, Singularities in virbo-impact dynamics, *Journal of Sound and Vibration* 152 (3) (1992) 427–460.

[11] S. Foale, S.R. Bishop, Dynamical complexities of forced impacting systems, *Philosophical Transactions of the Royal Society of London* 338 (A) (1992) 547–556.

[12] A.P. Ivanov, Stabilization of an impact oscillator near grazing incidence owing to resonance, *Journal of Sound and Vibration* 162 (3) (1993) 562–565.

[13] A.P. Ivanov, Bifurcation in impact systems, *Chaos, Solitons & Fractals* 7 (10) (1996) 1615–1634.

[14] F. Peterka, Bifurcation and transition phenomena in an impact oscillator, *Chaos, Solitons & Fractals* 7 (10) (1996) 1635–1647.

[15] F. Peterka, J. Vacik, Transition to chaotic motion in mechanical systems with impacts, *Journal of Sound and Vibration* 154 (1) (1992) 95–115.

[16] C. Budd, F. Dux, A. Cliffe, The effect of frequency and clearance variations on single-degree-of-freedom impact oscillators, *Journal of Sound and Vibration* 184 (3) (1995) 475–502.

[17] M.I. Feigin, The increasingly complex structure of the bifurcation tree of a piecewise-smooth system, *Journal of Applied Mathematics and Mechanics* 59 (6) (1995) 853–863.

[18] D. Bernardo, M.I. Feigin, S.J. Hogan, M.E. Homer, Local analysis of C-bifurcations in N-dimensional piecewise-smooth dynamical systems, *Chaos, Solitons & Fractals* 10 (11) (1999) 1881–1908.

[19] D.T. Nguyen, S.T. Noah, C.F. Kettleborough, Impact behaviour of an oscillator with limiting stops, part I: a parametric study, *Journal of Sound and Vibration* 109 (2) (1986) 293–307.

[20] S. Natsiavas, Dynamics of multiple-degree-of-freedom oscillators with colliding components, *Journal of Sound and Vibration* 165 (3) (1993) 439–453.

[21] S. Natsiavas, H. Gonzalez, Vibration of harmonically excited oscillators with asymmetric constraints, *Journal of Applied Mechanics* 59 (1992) 284–290.

[22] S. Chatterjee, A.K. Mallik, Bifurcations and chaos in autonomous self-excited oscillators with impact damping, *Journal of Sound and Vibration* 191 (4) (1996) 539–562.

[23] G.W. Luo, J.H. Xie, Hopf bifurcation of a two-degree-of-freedom vibro-impact system, *Journal of Sound and Vibration* 213 (3) (1998) 391–408.

[24] G. W. Luo, Doctor's degree dissertation, Southwest Jiaotong University, 1998.

[25] Hu Haiyan, Controlling chaos of a periodically forced nonsmooth mechanical system, *Acta Mechanica Sinica* 11 (3) (1995) 251–258.

[26] J.P. Mejaard, A.D. De Pater, Railway vehicle systems dynamics and chaotic vibrations, *International Journal of Non-Linear Mechanics* 24 (1) (1989) 1–17.

[27] L.A. Wood, K.P. Byrne, Analysis of a random repeated impact process, *Journal of Sound and Vibration* 78 (3) (1981) 329–345.

[28] S. Zhongzhou, S. Xiaozhen, Theoretical analysis of complete stability and automatic vibration isolation of impacting and vibrating systems with double masses, *Chinese Journal of Mechanical Engineering* 26 (3) (1990) 50–57.

[29] J.E. Kozol, R.M. Brach, Two-dimensional vibratory impact and chaos, *Journal of Sound and Vibration* 148 (2) (1991) 319–327.

[30] X. Jianhua, The mathematical model for the impact hammer and global bifurcations, *Acta Mechanica Sinica* 29 (4) (1997) 456–463.

[31] J.M.T. Thompson, Complex dynamics of compliant offshore structures, *Proceedings of the Royal Society of London Series A* 387 (1983) 407–427.
[32] C.K. Sung, W.S. Yu, Dynamics of harmonically excited impact damper: bifurcations and chaotic motion, *Journal of Sound and Vibration* 158 (2) (1992) 317–329.
[33] C.N. Bapat, C. Bapat, Impact-pair under periodic excitation, *Journal of Sound and Vibration* 120 (1) (1988) 53–61.
[34] P.R.S. Han, A.C.J. Luo, Chaotic motion of a horizontal impact pair, *Journal of Sound and Vibration* 181 (2) (1995) 231–250.
[35] M.S. Heiman, A.K. Bajaj, P.J. Sherman, Periodic motions and bifurcations in dynamics of an inclined impact pair, *Journal of Sound and Vibration* 124 (1) (1988) 55–78.
[36] C.N. Bapat, The general motion of an inclined impact damper with friction, *Journal of Sound and Vibration* 184 (3) (1995) 417–427.
[37] A. Kahraman, R. Singh, Non-linear dynamics of a geared rotor-bearing system with multiple clearances, *Journal of Sound and Vibration* 144 (3) (1991) 469–506.
[38] A. Kunert, F. Pfeiffer, Stochastic model for rattling in gear-boxes, in: W. Schiehlen (Ed.), *Nonlinear Dynamics in Engineering System*, Springer, Berlin, Heidelberg, 1990, pp. 173–180.
[39] G. Iooss, J.E. Los, Quasi-genericity of bifurcation to high dimensional invariant tori for maps, *Communications in Mathematical Physics* 119 (1988) 453–500.
[40] V.I. Arnol'd, *Geometrical Methods in the Theory of Ordinary Differential Equations*, Springer, Berlin, 1983.
[41] D.K. Arrowsmith, C.M. Place, *An Introduction To Dynamical Systems*, Cambridge University Press, Cambridge, 1990.
[42] J. Guckenheimer, P.J. Holmes, *Nonlinear oscillations, dynamical systems, and bifurcations of vector fields*, Second Printing, Springer New York, Berlin, Heidelberg, Tokyo, 1986.
[43] S. Wiggins, *An Introduction To Applied Nonlinear Dynamical Systems and Chaos*, Springer, Berlin, 1990.
[44] J. Carr, Applications of center manifold theory, In: *Applied Mathematical Sciences*, vol. 35, Springer, Berlin-Heidelberg, New York, 1981.
[45] J.E. Los, Non-normally hyperbolic invariant curves for maps in $\mathbf{R}^3$ and doubling bifurcation, *Nonlinearity* 2 (1) (1989) 149–174.
[46] B. D. Hassard, N.D. Kazarinoff, Y.H. Wan, *Theory and Applications of Hopf Bifurcation*, London Mathematical Society Lecture Note Series, 1981,Vol. 41.
[47] O.E. Landford, *Bifurcation of Periodic Solution Into Invariant Tori: The Work of Ruelle and Takens*, Lecture Notes in Mathematics, vol. 322, Springer, Berlin, 1973, pp. 159–192.
[48] B. Wen, F. Liu, *Theory and Application of Vibratory Mechanism*, Mechanism industry Press, Beijing, China, 1982.
[49] B. Wen, Y. Li, Q. Han, *Theory and Application of Nonlinear Oscillation*, Northeast University Press, Shenyang, China, 2001.